BRNO UNIVERSITY OF TECHNOLOGY

VYSOKÉ UČENÍ TECHNICKÉ V BRNĚ

FACULTY OF ELECTRICAL ENGINEERING AND COMMUNICATION

FAKULTA ELEKTROTECHNIKY
A KOMUNIKAČNÍCH TECHNOLOGIÍ

DEPARTMENT OF ELECTRICAL AND ELECTRONIC TECHNOLOGY

ÚSTAV ELEKTROTECHNOLOGIE

TESTING OF A PROTOTYPE DEVICE USING ELECTROCHEMICAL IMPEDANCE SPECTROSCOPY (EIS)

TESTOVÁNÍ PROTOTYPOVÉHO ZAŘÍZENÍ VYUŽÍVAJÍCÍ METODU ELEKTROCHEMICKÉ IMPEDANČNÍ SPEKTROSKOPIE (EIS)

MASTER'S THESIS

DIPLOMOVÁ PRÁCE

AUTHOR — **Bc. András Zsigmond**

AUTOR PRÁCE

SUPERVISOR — **Ing. Jiří Libich, Ph.D.**

VEDOUCÍ PRÁCE

BRNO 2019

BRNO UNIVERSITY OF TECHNOLOGY
FACULTY OF ELECTRICAL ENGINEERING AND COMMUNICATION

Master's Thesis

Master's study field **Electrical Manufacturing and Materials Engineering**
Department of Electrical and Electronic Technology

Student: Bc. András Zsigmond ***ID:*** 154915

Year of study: 2 ***Academic year:*** 2018/19

TITLE OF THESIS:

Testing of a Prototype Device Using Electrochemical Impedance Spectroscopy (EIS)

INSTRUCTION:

Familiarize yourself with lithium-ion batteries, their characteristics, operating principle and their use in conventional applications. Focus on the lithium-ion cell as a whole, and study its behavior, in particular the general causes that lead to degenerative changes resulting in deterioration of the battery electrochemical parameters. Study the correlation of these changes with the changes in internal battery impedance. Use the method of electrochemical impedance spectroscopy (EIS) to analyze these parameters. Compare the results of EIS analysis obtained with a conventional commercial equipment and the tested prototype. Compare and evaluate the results. Evaluate the effect of internal impedance on lithium-ion battery parameters.

RECOMMENDED LITERATURE:

Podle pokynů vedoucího práce.

Date of project specification: 4.2.2019 ***Deadline for submission:*** 21.5.2019

Supervisor: Ing. Jiří Libich, Ph.D.
Consultant:

doc. Ing. Petr Bača, Ph.D.
Subject Council chairman

Abstract

This diploma thesis deals with the electrochemical processes in lithium-ion batteries. To characterize the different electrochemical processes a method called electrochemical impedance spectroscopy (EIS) is used. In the first couple of chapters the different types of batteries and their differences are described. The thesis also contains the description of an experimental device used for EIS. The thesis also contains a comparison between the experimental device and the device from BioLogic Science Instruments.

Keywords

lithium, battery, negative electrode, capacity, electrochemical, impedance, EIS

Abstrakt

Tato diplomová práce se zabývá elektrochemickými procesy v lítium-iontových bateriích. Pro charakterizaci různých elektrochemických procesů se používá metoda nazývaná elektrochemická impedanční spektroskopie (EIS). V prvních kapitolách jsou popsány různé typy baterií a jejich rozdíly. Práce také obsahuje popis experimentálního zařízení používaného pro EIS. Součástí práce je také porovnání experimentálního zařízení a zařízení od společnosti BioLogic Science Instruments.

Klíčová slova

lítium, baterie, záporná elektroda, kapacita, elektrochemická, impedance, EIS

ZSIGMOND, András. *Testing of a Prototype Device Using Electrochemical Impedance Spectroscopy (EIS)*. Brno, 2019. Dostupné také z: https://www.vutbr.cz/studenti/zav-prace/detail/119390. Master's Thesis. Vysoké učení technické v Brně, Fakulta elektrotechniky a komunikačních technologií, Department of Electrical and Electronic Technology. Supervisor Jiří Libich.

Author's statement on the originality of the work

I declare that I have written my diploma thesis "*Testing of a Prototype Device Using Electrochemical Impedance Spectroscopy (EIS)*" independently, under the guidance of the doctoral thesis supervisor and using the technical literature and other sources of information which are all quoted in the thesis and detailed in the list of literature at the end of the thesis.

As the author of the diploma thesis, I furthermore declare that, as regards the creation of this doctoral thesis, I have not infringed any copyright. In particular, I have not unlawfully encroached on anyone's personal and/or ownership rights and I am fully aware of the consequences in the case of breaking Regulation §11 and the following of the Copyright Act No. 121/2000 Coll., and of the rights related to intellectual property right and changes in some Acts (Intellectual Property Act) and formulated in later regulations, inclusive of the possible consequences resulting from the provisions of Criminal Act No. 40/2009 Coll., Section 2, Head VI, Part 4.

Brno ....

(signature)

Contents

List of images

List of Tables

INTRODUCTION

Batteries exist since the end of the 19th century. They provided the main source of electricity before the development of electric generators. Successful improvements in battery technology lead us to the use of portable computers, mobile phones, electric cars, and many other electrical devices.

The term "battery" was first used by Benjamin Franklin in the 18th century. He described a set of linked capacitors as a "battery". These capacitors were panels of glass coated with metal on each surface and were charged with an electrostatic generator and discharged by touching metal to their electrodes. The term originally meant "a group of two or more similar objects functioning together". Later on this term was used for voltaic piles and similar devices similar to Franklin's connected capacitors. Today even a single electrochemical cell is called a battery.

Experimentation with lithium batteries began in 1912 by G.N. Lewis, and in the 1970s the first lithium batteries were sold. Important developments were made in the 1980s. An American chemist John B. Good experimented with $LiCoO_2$ as the positive electrode (cathode). Another research scientist Rachid Yazami at the same time discovered the graphite anode (negative electrode). The results of these experiments were put together by Akira Yoshino of Asahi Chemical in Japan. The first lithium-ion battery prototype was built in 1985. The commercialization of the lithium-ion battery was done by Sony in 1991. [1]

1 BATTERIES

Battery is a device used to store electric energy. It changes chemical energy to electricity by putting certain chemicals in contact with each other in a specific way. When electrons flow, this makes an electrical current that can power a lot of different devices, mobile phones, e-cigarettes, remote controls, etc. [2]

Batteries have three parts, a negative electrode (*anode* -), a positive electrode (*cathode* +), and the *electrolyte*. The positive electrode and negative electrode is used to connect the battery to an electrical circuit. The chemical reactions in the battery cause a buildup of electrons at the negative electrode. This results in an electrical difference between the two electrodes. The electrons want to rearrange themselves to get rid of this difference. Electrons repel each other and try to go to a place with fewer electrons, the only place to go is to the positive electrode. The electrolyte keeps the electrons from going straight from the negative to the positive electrode within the battery. When the circuit is closed the electrons will be able to get to the positive electrode through the electrical circuit. [2]

1.1 Lithium-ion batteries

Work with the lithium battery (LIB) began in 1912 but it was not until the early 1970s when the first non-rechargeable lithium batteries became commercially available. The use of lithium metal was not possible due to the instability of the material, especially during charging. Research shifted to a non-metallic lithium battery using lithium ions. In comparison lithium-ion is more stable than pure lithium, however it is lower in energy density. [3]

Figure 1.1 Lithium-ion batteries [7]

Figure 1.1 shows the various shapes of the Li-ion batteries. These can be divided into four groups. Small cylindrical, which has a solid body without terminals and can be used in laptop batteries. Large cylindrical with solid body and large threaded terminals. Batteries with soft, flat body called pouch. These are mainly used in cell phones. The fourth type is a semi-hard plastic case with large threaded terminals, called prismatic and they are used as vehicle traction packs. [5]

The primary components of a lithium-ion battery are the positive and negative electrodes, the separator and the electrolyte. The negative electrode is generally made from carbon, while the positive electrode is metal oxide. Lithium salt in an organic solvent is used as the electrolyte. Depending on the direction of current flow the electrochemical roles of the electrodes reverse between anode and cathode. The most popular material used as the negative electrode is graphite. The positive electrode is either, layered oxide (lithium cobalt oxide), a polyanion (lithium-iron phosphate) or spinel (lithium-manganese oxide). [5]

As mentioned before the electrolyte is a mixture of organic carbonates (ethylene carbonate or diethyl carbonate) containing lithium ions. These non-aqueous electrolytes use anion salts such as lithium hexafluorophosphate ($LiPF_6$), lithium hexafluoroarsenate monohydrate ($LiAsF_6$), lithium perchlorate ($LiClO_4$), lithium tetrafluoroborate ($LiBF_4$) and lithium triflate ($LiCF_3SO_3$). The reason why non-aqueous electrolytes are used lays in the highly reactive properties of lithium. The reaction with water produces lithium hydroxide and hydrogen gas, therefore the sealed container strictly excludes moisture from the battery pack. Material choices heavily affect the voltage, energy density, life and safety of a lithium-ion battery. Performance improvements have been employed by new architectures using nanotechnology. [5]

When the battery is charging up, the lithium-cobalt oxide, positive electrode gives up some of its lithium ions. These ions move through the electrolyte to the negative, graphite electrode. The battery takes in and stores energy during this process. When the battery is discharging, the lithium ions move back to the positive electrode, producing the energy. In both cases, electrons flow in the opposite direction to the ions around the outer circuit. Electrons do not flow through the electrolyte, it is an insulating barrier. The movement of ions and electrons are connected, if either one of them stops so does the other. Ions can stop moving through the electrolyte if the battery completely discharges, if that happens then the electrons can't move through the circuit, the battery loses power. Similarly, if the device powered by the battery is switched off, the flow of electrons stops and so does the flow of ions. [5]

Unlike simpler batteries, lithium-ion batteries have built in electronic controllers that regulate how they charge and discharge. They prevent the overcharging and overheating that can cause lithium-ion batteries to explode. [5]

Lithium is a highly reactive element; a lot of energy can be stored in its atomic bonds. Typically lithium-ion batteries can store 150 watt-hours of electricity in 1 kilogram of battery. A Ni-MH (nickel-metal hydride) battery pack can store typically 60 to 70 watt-hours in 1 kilogram of battery, while a lead-acid battery can store only 25 watt-hours per kilogram. Using lead-acid technology means that, it would take 6 kilograms to store the same amount of energy that a 1 kilogram lithium-ion battery can handle. Other important advantages are related to charge. A lithium-ion battery pack loses only about 5 % of its charge per month, compared to a 20 % loss per month for Ni-MH batteries. They have no memory effect, which means that it does not have to be completely discharged before recharging. They can handle hundreds of charge/discharge cycles. [5]

Of course lithium-ion batteries have some flaws. They start degrading as soon as they leave the factory. They will only last a few years whether it is used or not. They are extremely sensitive to high temperatures. Heat causes lithium-ion battery packs to

degrade much faster than they normally would. If it's completely discharged they are ruined. A lithium-ion battery pack must have an on-board computer to manage the battery. This makes them more expensive. There is a small chance that, if a lithium-ion battery pack fails, it will burst into flame. [5]

1.2 Cathode material

In the beginning of development $LiCoO_2$ (LCO) was the dominant cathode material, with the spinel $LiMn_2O_4$ (LMO) occupying only a small part of the market. Over time the LCO remained the most common cathode material, however the market has been flooded by other materials. By 2010, the use of $LiNi_{1/3}Mn_{1/3}Co_{1/3}O_2$ (NMC), a ternary system with nickel, manganese, and cobalt, had increased. For certain applications the use of $LiNi_{0,8}Co_{0,15}Al_{0,05}O_2$ (NCA) and LMO are preferred. With only a limited use, phosphates with an olivine structure is a promising new class of cathode materials, $LiFePO_4$ (LFP) being the most prominent. [6]

1.3 Anode material

The discharge profile for lithium-ion battery anode made of graphite, has a curve characterized by a very broad, flat range (shown in Figure 1.2). For hard carbon the discharge profile is characterized by a steadily declining curve across the charge range, shown in Figure 1.3. For the rapidly spread mobile phones a flat discharge profile is preferable, meaning graphite became the dominant anode material. Among the various types of graphite, modified natural graphite has become the most common. Mostly because natural graphite is inexpensive, available, however its high reactivity to electrolyte prevents its use without modification. The most widely used technology is to coat the graphite surface with thin carbon layer. A more recent development in the anode market is the resurgence of hard carbon. It is making a comeback, due to its suitable use for HEV applications. [6]

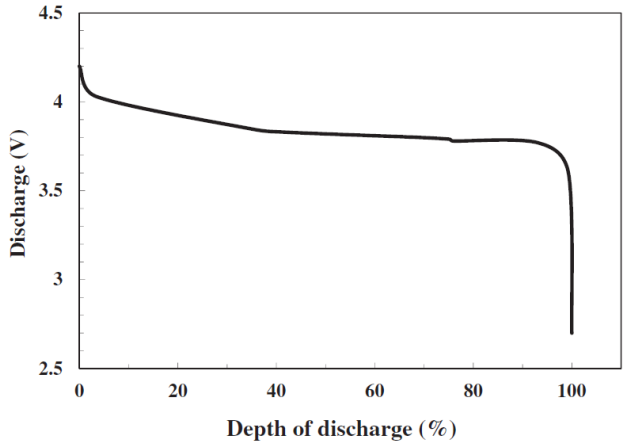

Figure 1.2 Discharge curve with a graphite anode [6]

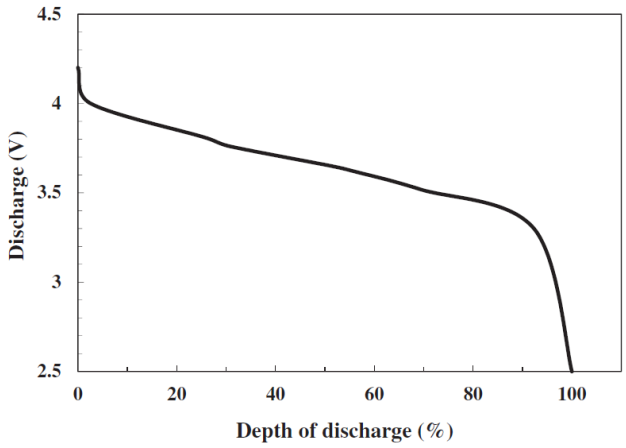

Figure 1.3 Discharge curve with a hard carbon anode [6]

1.4 Electrolyte solutions

The electrolyte for LIBs is a mixture of organic solvents and an electrolyte salt compound, most commonly mixtures of cyclic carbonate esters (ethylene carbonate, propylene carbonate), and linear carbonate esters (dimethyl carbonate, diethyl carbonate). The added salt compound is commonly $LiPF_6$ or $LiBF_4$. The free transport of lithium ions requires high dielectric constant and low viscosity. The required dielectric constant and viscosity can be achieved by mixing cyclic carbonate esters and linear carbonate esters. [6]

1.5 Separators

The separator in lithium-ion batteries is a thin microporous membrane made of polyolefin. It is used to prevent contact between the anode and cathode, while enabling lithium ions to pass through. The three basic categories of separator are classified based on their production methods, with different morphologies and characteristics, each for different battery applications. The typical separators produced by each of the three methods are shown in Figure 1.7. [6]

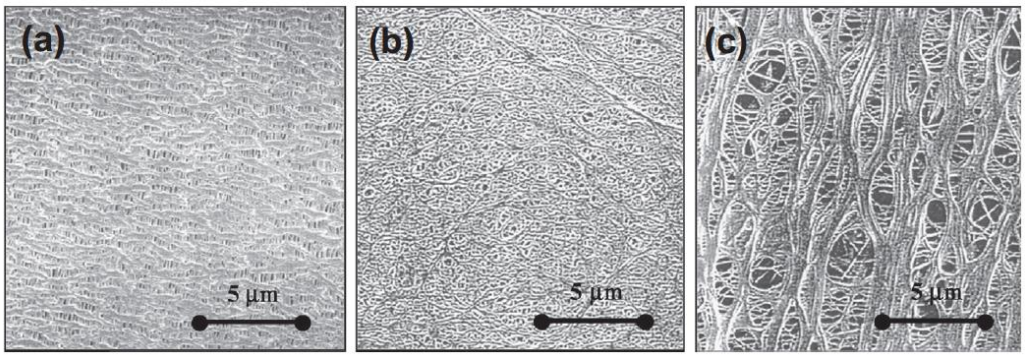

Figure 1.4 Pore characteristics (a) Dry-process one-component system (b) wet-process two-component system and (c) wet-process three-component system [6]

2 ELECTROCHEMICAL REACTIONS

This chapter contains the description of chemical reactions occurring in one battery cell. A schematic diagram of the cell is shown providing visual information about the chemical reactions, which are also described by chemical equations. The forming of the solid electrolyte interphase (SEI) is also described in this chapter.

2.1 Reactions in a lithium-ion cell

Figure 2.1 shows a schematic diagram of a lithium-ion cell. The positive electrode is made of lithium metal oxide ($LiMO_2$), where M stands for a metal such as Co, while the negative electrode is lithiated carbon (LixC). The active materials are connected to current collectors at both ends of the cell. The electrolyte between the active materials is electrically isolating and they are usually made of a microporous polymer or gel-polymer. Liquid or gel-polymer electrolytes enable lithium ions (Li^+) to diffuse between the positive and negative electrodes. The lithium ions are inserted into or de-inserted from the active materials through an intercalation process. [8]

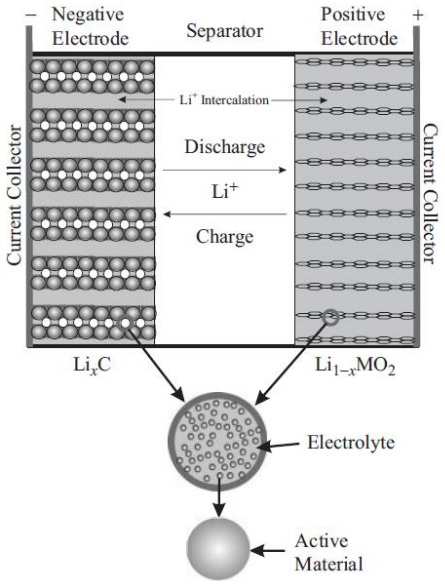

Figure 2.1 Schematic diagram of lithium-ion cell [8]

During charge in the positive electrode the active material is oxidized and lithium ions are de-intercalated:

$$Li_{1-x}CoO_2 + xLi^+ + xe^- \xleftarrow{charge} \xrightarrow{discharge} LiCoO_2 \text{ . [8]} \qquad (2.1)$$

In the negative electrode during charge, the active material is reduced and the lithium ions that migrate from the positive electrode are intercalated in the reaction:

$$Li_xC \xleftarrow{charge} \xrightarrow{discharge} C + xLi^+ + xe^- \text{ . [8]} \qquad (2.2)$$

These reactions produce a theoretical cell voltage of 4,1 V, which is a higher value than the Ni-MH (Nickel-metal hydride) or lead-acid cells. The capacity of a lithium-ion battery fades with cycling. This is due to the increase of internal resistance or

impedance. Thanks to these Ohmic losses, energy is wasted, heat is produced and the aging is accelerated. Losses in capacity can also be caused by the degradation of the positive and negative electrodes and the electrolyte. The degradation mechanisms are dependent on cell chemistry, design and manufacturing. In the negative electrode, the dominant aging mechanisms are: SEI growth, lithium corrosion, contact loss and lithium plating. [8]

The growth of the SEI leads to an impedance rise and the entraining of lithium atoms. The SEI layer forms at the beginning of cycling and grows during cycling and storage, especially at higher temperatures. Lithium corrosion causes capacity fade due to the irreversible loss of lithium. The corroding lithium is found in the active carbon material of the negative electrode. Contact loss means that the impedance of the cell increases by the disconnection of the SEI layer from the negative electrode. If the cell is at low temperatures with high charge rates, the lithium metal can plate on the negative electrode. This leads to irreversible loss of lithium. [8]

Recent studies show that impedance rise and capacity fade can be caused by the positive electrode. The rise in impedance and the capacity fade primarily happens during cycling. The discharge capacity may be limited by a decrease in active lithium intercalation sites in the oxide particles. A passivation layer also forms on the positive electrode which can change properties during cycling, resulting in cell impedance rise and power fade. [8]

2.2 Forming of the SEI layer

SEI is an ionically conductive, electrically not conductive polymer layer. A schematic representation is shown in Figure 2.2. This layer is created at the first formation by a strong reaction between the carbon anode and the electrolyte, which requires about 15-45 % of the total battery capacity. Maintaining stability, reduction of fluctuations during charging or temperature fluctuations is among the main characteristics of this layer, together with an effect on overall battery life. The thickness of the SEI layer varies over time. The increase in thickness contributes to a reduction in capacity. In materials that have a higher charge/discharge potential than lithium, the SEI layer thickness is much smaller. On the surface of materials like the LTO (where the charge/discharge potential is 1,55 times bigger than lithiums) the SEI layer is very thin, it can almost be completely ignored. [9]

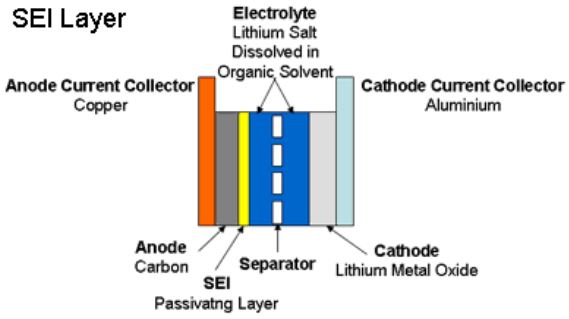

Figure 2.2 SEI layer [2]

The major components of SEI layer are degraded products of electrolyte solvents

and salts, which were identified by using spectroscopic analysis. The mentioned degraded products include Li_2CO_3, lithium alkyl carbonate, lithium alkyoxid and other groups of salts, such as LiF. Based on the layer composition two mechanisms were identified in the formation process while using an electrolyte with carbon solvents. An example of the SEI layer formation in an ethyl carbonate (EC) solvent is shown in Figure 2.3. [9]

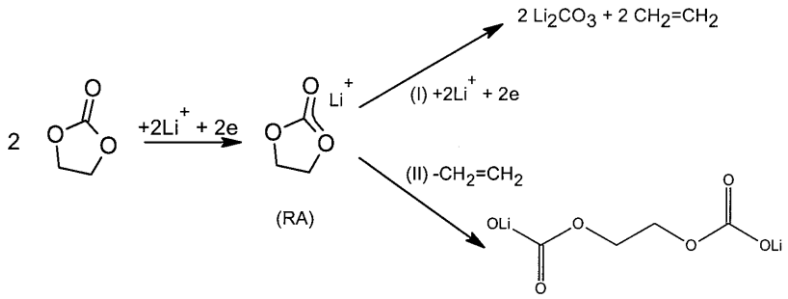

Figure 2.3 Formation of the SEI layer in EC solvent [9]

Acronym RA in the figure means radical anion; it's the reactive compound in the solution. The formation of the SEI layer happens with both reactions present, as seen in the figure. With the domination of mechanism (I) the decomposition of the compound generates gaseous products, resulting in less stable Li_2CO_3 as the final layer. Mechanism (II), on the other hand, generates less gaseous products, forms a layer insoluble in the electrolyte. Another advantage of mechanism (II) is greater stability in the battery. These two mechanisms involved in the formation of SEI layer also depend on the graphite surface morphology. The layer formed on the edges of the surface is oriented towards pyrolytic graphite and is rich in inorganic compounds. In contrast, the middle layer is formed predominantly by organic compounds. [9]

The creation of the SEI layer can also be categorized into two stages. The first stage takes place before the intercalation of lithium ions into the graphite. This results in a structurally porous, highly resistive and dimensionally unstable layer. At the end of the second stage the layer is formed by the intercalation of lithium, producing a more compact and highly conductive layer. The capacity created in the second stage is connected not only to the reduction of the solvent molecules, but to the electrochemical reduction of functional surface groups on the side of the graphite as well. [9]

2.3 Additives for improving the SEI layer

The SEI layer formed before the intercalation of lithium is unstable and full of inorganic compounds. Furthermore, the formation is accompanied by the generation of gas. A possible method for suppressing this layer is done with a chemical coating on the graphites surface by a layer of organic film. These types of additives have a higher reduction potential than electrolytic solvents, and are selected because they are insoluble and protect the surface of the graphite against reaction within the electrolyte. Reduced generation of gas and an increased overall stability can be achieved with the use of these additives. Figure 2.4 shows possible additives, containing one or more double carbon-carbon bonds. [9]

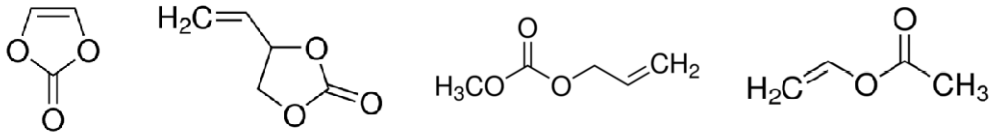

Figure 2.4 The chemical structures of the additives: a.) vinyl carbonate, b.) vinyl ethylene carbonate, c.) allyl ethyl carbonate, d.) vinyl acetate [9]

During the creation of the SEI layer the products of reducing agents are absorbed into the graphite. The effectiveness of facilitating the formation of the layer depends on the molecular groups. These groups can help create the layer; they belong to the group of sulfuric compounds, including SO_2, CS_2 and others. Sulfuric compounds are not soluble in organic electrolytes and are unstable at higher potentials, resulting in self-discharge. This means that the amount of sulfuric additive has to be limited. Other usable types of reducing agents contain nitrogen, such as N_2O. [9]

The next type of additive is capable of devouring radical anions, which are undesirable solvents, or can combine products such as lithium alkyl dicarbonate, thereby creating a more stable SEI layer. The above mentioned improvements can be done with CO_2. Instead of CO_2 dialkyl pyrocarbonate is a possible additive, with a weaker solubility and higher pressure, capable of reaching higher conductivity within the SEI layer under lower temperatures. Other types of reagents, certain boron compounds increase the life of the battery, while LiBOB increases high-temperature parameters. [9]

Salts of alkali metals reduce the irreversible capacity, improving the holding of the capacity during cycling. SEI layer formed in the presence of Na_2CO_3 has a higher conductivity. The results of pretreated graphite in a solution containing Na_2CO_3 is shown in Figure 2.5. This figure shows reduced irreversible capacity and reduced possibility for Li^+ intercalation and de-intercalation in the graphite structure. [9]

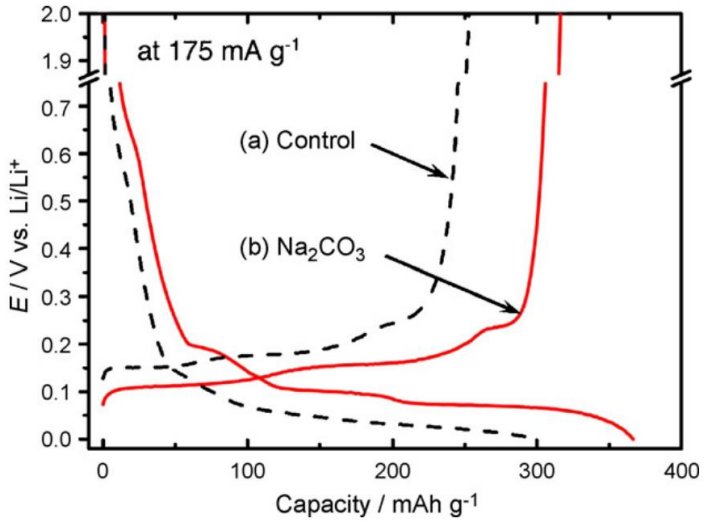

Figure 2.5 Characteristics of the graphite, (a) without pretreatment, (b) pretreatment with Na2CO3 [9]

3 PERFORMANCE COMPARISON

This chapter contains the comparison between the most popular types of batteries. For each type of battery (lead-acid, nickel-metal hydride and lithium-ion batteries) a description about the energy density, charge and discharge characteristics, cycle life and information about the temperature operating range is included.

3.1 Energy density and specific energy

The key categories of the comparison are shown in Table 3.1. The electrode materials determine the theoretical voltage, while the practical voltage is what can be achieved in a real battery. For lead-acid and lithium-ion batteries the practical values and the theoretical values are essentially the same, however the nickel-metal hydrnide (Ni-MH) batteries show a 10% difference. Following the previous values the specific energy is listed, which is the energy storage capacity in watt-hours (Wh) divided by the mass of the battery in kilograms (kg). Equivalent weight of the active materials participating in the electrochemical reaction determines the theoretical capacity in ampere-hours/gram (Ah/g). Multiplying the theoretical capacity and voltage gives the theoretical specific energy in Wh/kg. [8]

Table 3.1 lists a number of properties, and in most of them the lithium-ion battery excels over the lead-acid and nickel-metal hydride batteries.

Table 3.1 Comparison of lithium-ion, lead-acid and nickel-metal hydride performance [8]

	lithium-ion	**nickel-metal hydride**	**lead-acid**
Theoretical			
Voltage [V]	4,1	1,35	1,93
Specific energy [Wh/kg]	410	240	166
Practical			
Specific energy [Wh/kg]	150	75	35
Energy density [Wh/L]	400	240	70
Coulometric efficiency	>0,85	0,65 - 0,70	0,80
Energy efficiency	~0,80	0,55 - 0,65	0,65 - 0,70
Specific power, 80% DOD [W/kg]	350	150	220
Power density [W/L]	>800	>300	450

An important metric for batteries, listed in Table 3.1, is the energy storage efficiency. This can be determined by two metrics: coulometric efficiency and energy efficiency. Coulometric efficiency:

$$f = \frac{\int_{discharge} Idt}{\int_{charge} Idt}, \tag{3.1}$$

where I (t) is the battery current and t is time. Energy efficiency:

$$\eta = \frac{\int_{discharge} IUdt}{\int_{charge} IUdt}, \tag{3.2}$$

where V(t) is the battery voltage. Lithium-ion has the most efficient chemistry followed by lead-acid and nickel-metal hydride. [8]

3.2 Charge and discharge

Charge and discharge operation regulates the speed of current put into and taken from storage, this is called dynamic performance. The terminal voltage rises and falls during steady charging and discharging. At the end of charging or discharging the transient voltage response settles out, for sufficient long charges, the battery voltage saturates at a maximum value. These are overcharged situations, where most of the input energy goes to heat losses or harmful side reactions. [8]

Similarly, undercharge occurs when the battery voltage falls below the end or cut-off voltage causing damage to the battery. The state of charge (SOC), defined as the percentage of maximum possible charge that is present inside a rechargeable battery, determines the working range of a battery. A fully charged battery is at 100 % SOC, however a more practical example would be 30 to 70 % SOC with a Ni-MH battery in hybrid electric vehicle (HEV) applications having a very high coulometric efficiency. The depth of discharge (DOD = 100 % - SOC) is another way to quantify stored charge. [8]

The rate of charge or discharge is measured relative to the battery capacity C, meaning that a 0,1 C discharge rate for a 5 Ah battery is 0,5 A or a 2 C discharge rate for a 10 Ah battery is 20 A. Figure 3.1 shows discharge plots at low, medium, and high rates. [8]

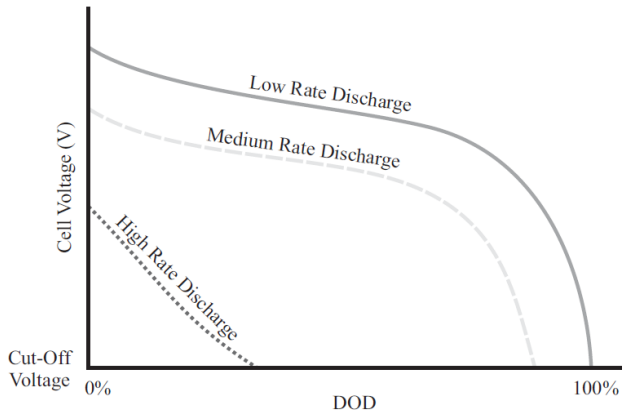

Figure 3.1 Example voltage curves for different discharge rates [8]

The low rate curve approximates the equilibrium cell (or open-circuit) potential. For the voltage to remain constant during discharge the optimal open-circuit potential curve is flat over a broad range of DOD. This simplifies the design and reduces the cost of the added voltage-regulation circuits. Due to Ohmic losses over the entire DOD

range the medium rate discharge curve shifts downward. Charge transfer kinetic losses and mass transport limitations at low and high DOD are also responsible for the discharge curve to shift downward. [8]

The high rate discharge case demonstrates that only a fraction of the capacity can be utilized at high discharge rates due to quick voltage drops. A good way to summarize the statistics for battery discharge performance is with specific power (W/kg) and power density (W/L). These values are shown in Table 3.1, where lithium-ion has the highest specific power and power density. [8]

3.3 Cycle life

The most reliable way to determine cycle life is to test several batteries from the same batch. Test results depend on battery chemistry, discharge-charge cycle, temperature, prior history of storage and manufacturer, and are conducted on a cycling machine that repeats a prescribed current trajectory representing a typical cycle. During the testing process one of the batteries is randomly selected from cycling to be tested for capacity. This way, a plot of capacity versus number of cycles can be obtained. Generally all batteries have longer life for lower depths of discharge (DOD) cycles. At 100 % DOD Li-ion batteries typically last 3000 cycles at low charge/discharge rates and room temperature. A 20-40 % DOD, however can last 20 000 cycles. Other types of batteries, like the nickel-metal hydride and lead-acid batteries only last a few hundred cycles at 80-100 % DODs. The end of life is characterized by a drop in capacity by 50-80% from the initial capacity, depending on the chemistry and application. [8]

3.4 Temperature operating range

The use of batteries at extremely low or high temperatures is not optimal. Problems occurring at low temperature are tied to ionic diffusion and migration with possible lithium plating. The battery used in higher temperatures is exposed to corrosion and gas generation. For lithium-ion and lead-acid batteries, charge and discharge temperatures should be between -40 and 60 °C. The operating range for nickel-metal hydride batteries is a bit narrow; it's between -20 and 45 °C. [8]

4 ELECTROCHEMICAL IMPEDANCE SPECTROSCOPY (EIS)

This is an experimental technique for investigating the volume and interphase electrical properties of various types of solid or liquid materials. The method is based on measuring the complex impedance in frequency response, with an applied low-amplitude sinusoidal signal.

The system is usually measured over a wide range of frequencies to detect both fast (charge transfer) and slow (diffuse) electrode events. It is recommended to start measuring from higher frequencies to lower, as some systems are limited in stability. Frequencies range from 1 MHz to 0.1 mHz. An important advantage of electrochemical impedance spectroscopy is the possibility of applying frequencies gradually; this is the so-called single-sine technique. With this method the measured values have higher accuracy. The condition of proper measurements depends on the choice of the appropriate amplitude. Too high amplitude values can cause irreversible changes in the material. Low amplitude may be distorted by noise. [8]

Impedance Z describes the complex resistance. The voltage is applied to the electrode and the current response is measured, which according to Ohm's law means the resistance of the system. Since alternating voltage is used, the resistance is frequency dependent and is called impedance. The properties of the electrical elements can be determined from the frequency dependency, described by the phase shift between voltage and current. [8]

The more commonly applied method is the potentiostatic. With this method the electrochemical impedance is measured by applying an AC potential to an electrochemical cell and then measuring the current through the cell. If the applied signal is a sinusoidal potential excitation, the response is going to be an AC current signal. Electrochemical impedance is normally measured using a small excitation signal, so that the cell's response is linear (pseudo-linear). In a system like this, the current response will be a sinusoid signal shifted in phase. [8]

The excitation signal is expressed as a function of time:

$$U_t = U_0 \sin(\omega t), \tag{4.1}$$

where U_t is the potential at time t, U_0 is the amplitude of the signal, and ω is the radial frequency. The response signal, It, is shifted in phase (ϕ):

$$I_t = I_0 \sin(\omega t + \phi). \tag{4.2}$$

With the help of (4.1) and (4.2) the impedance Z will be described by its magnitude, Z_0, and a phase shift, ϕ:

$$Z = \frac{U_t}{I_t} = \frac{U_0 \sin(\omega t)}{I_0 \sin(\omega t + \phi)} = Z_0 \frac{\sin(\omega t)}{\sin(\omega t + \phi)}. \tag{4.3}$$

Before the availability of modern EIS instrumentation analysis of Lissajous Figures (sinusoidal signal U(t) plotted on the X-axis of a graph, the response signal I(t) plotted on the Y-axis) on oscilloscope screens was the accepted method of impedance

measurement. With the help of Eulers relationship,

$$\exp(j\phi) = \cos\phi + j\sin\phi, \tag{4.4}$$

it is possible to express the impedance as a complex function.

$$U_t = U_0 \exp(j\omega t), \tag{4.5}$$

$$I_t = I_0 \exp(j\omega t - \phi). \tag{4.6}$$

The impedance is then represented as a complex number:

$$Z = \frac{U}{I} = = Z_0 \exp(j\phi) = Z_0(\cos\phi + j\sin\phi). \tag{4.7}$$

The other method is the galvanostatic. It is the less commonly used method. The principle is the opposite of the potentiostatic method. A constant DC current with superimposed low amplitude alternating current is fed to the working electrode. The alternating voltage component is measured. [11]

4.1 Data presentation

The expression for Z is composed of a real and an imaginary part. These parts are plotted on a chart and it's called a Nyquist Plot (Figure 4.1). The real part is plotted on the X-axis and the imaginary part is plotted on the Y-axis.

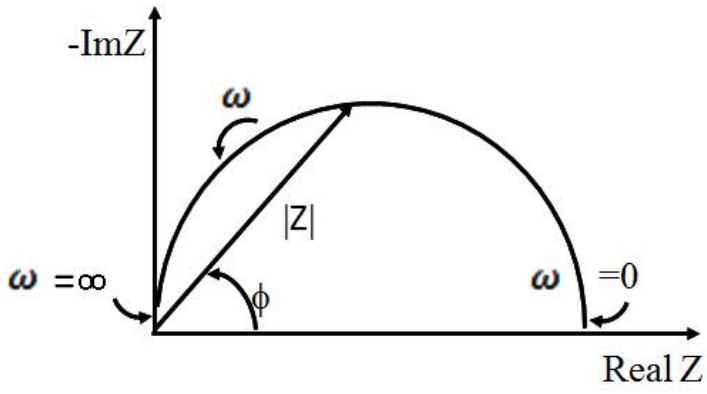

Figure 4.1 Nyquist Plot with Impedance Vector [11]

The impedance |Z| is represented as a vector (arrow). The angle ϕ is called phase angle. One major shortcoming in the Nyquist Plot is that it cannot be determined what frequency was used to record the data points.

Another popular presentation method is the Bode Plot. The impedance is plotted with log frequency on the X-axis and both the absolute values of the impedance ($|Z|=Z_0$) and the phase-shift on the Y-axis. Unlike the Nyquist Plot, the Bode Plot does show frequency information. [11]

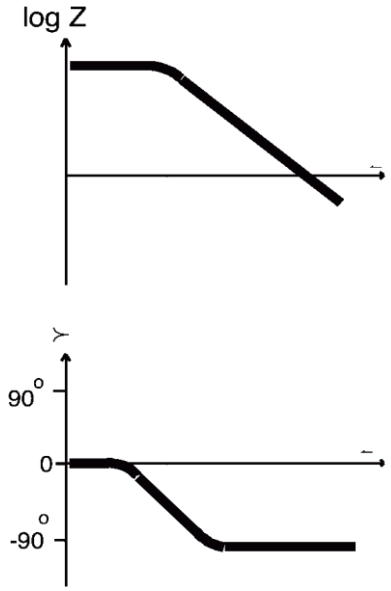

Figure 4.2 Bode Plot with One Time Constant [11]

4.2 Electrical circuit elements

Determining of the electrical properties of the system is done by approximating the model of the equivalent circuit. Most of the circuit elements in the model are common electrical elements such as resistors, capacitors, and inductors. Most models contain a resistor that models the cell's solution resistance. [11]

Table 4.1 Common Electrical Elements [11]

component	current vs. voltage	impedance
resistor	$U = I.R$	$Z = R$
inductor	$U = L.\frac{di}{dt}$	$Z = j\omega L$
capacitor	$I = C.\frac{du}{dt}$	$Z = \frac{1}{j\omega C}$

The impedance of a resistor is independent of frequency and has no imaginary components; therefore the current through a resistor stays in phase with the voltage. Inductors have only an imaginary impedance component, the current through an inductor is phase-shifted -90 degrees with respect to the voltage. Capacitors also have only an imaginary impedance component. The current through a capacitor is phase shifted 90 degrees with respect to the voltage. Few electrochemical cells can be modeled using a single equivalent circuit element, EIS models usually consist of a number of elements in a network. Both serial and parallel combinations of elements can occur. [11]

4.2.1 Common Equivalent Circuit Models

Some of the common equivalent circuit models can be used to interpret simple EIS data. Many of these models have been included as standard models in different EIS software. The most common elements are presented in Table 4.2. Equations for both the admittance and impedance are given for each element.

Table 4.2 Circuit Elements Used in the Models [11]

equivalent element	admittance	impedance
R	$\frac{1}{R}$	R
C	$j\omega C$	$\frac{1}{j\omega C}$
L	$\frac{1}{j\omega L}$	$j\omega L$
W (infinite Warburg)	$Y_0\sqrt{j\omega}$	$\frac{1}{Y_0\sqrt{j\omega}}$
O (finite Warburg)	$Y_0\sqrt{j\omega}.\coth(B\sqrt{j\omega})$	$\frac{\tanh(B\sqrt{j\omega})}{Y_0\sqrt{j\omega}}$
Q (CPE)	$Y_0(j\omega)^{\alpha}$	$\frac{1}{Y_0(j\omega)^{\alpha}}$

The EIS software uses the following variables as fit parameters, R, C, L, Y_0, B, and α. B is a constant and α is an exponent equaling 1 for a capacitor. [11]

4.3 A typical representation of a fuel cell

The above mentioned circuit elements can express the properties of the fuel cell, such as the properties of the three major parts: anode, electrolyte and cathode. Resistance characterizes the transport of ions or electrons. In Figure 4.3 the electrolyte section is being shown as a resistance model with small resistances in the anode and cathode part to account for the resistance of electron movement. [12]

An electrical double layer exists at the interface between an electrode and the surrounding electrolyte. Charges in the electrode are separated from the charges of the ions in the solution. This separation is very small (order of nanometers) and form a capacitor. The value of the double layer capacitance depends on electrode potential, temperature, ionic concentrations, types of ions, oxide layers, electrode roughness, impurity adsorption, etc. Figure 4.3 shows these capacitors on both sides. The Warburg element accounts for the diffusion layer formed at the cathode section. It resists the flow of hydronium ions to the cathode. [12]

A representative Nyquist plot for a fuel cell is on the lower part of Figure 4.3. The values in the Figure are just examples taken from [12].

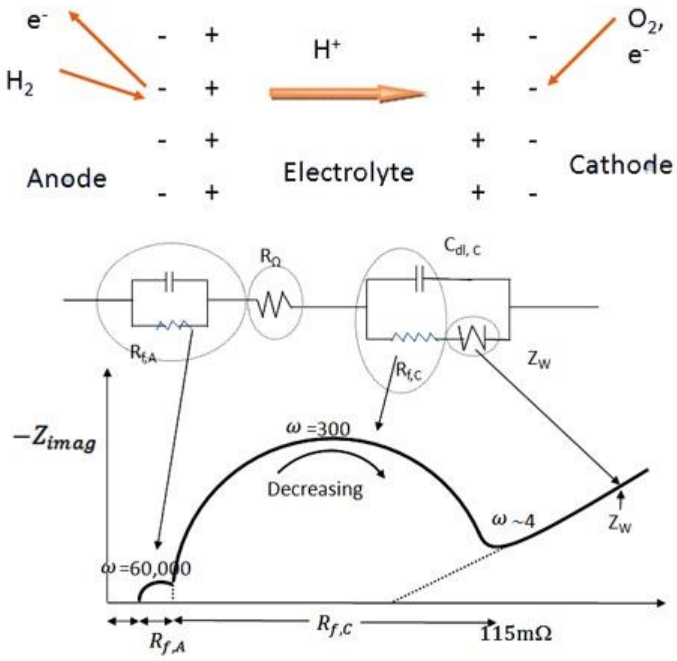

Figure 4.3 A typical representation of a fuel cell [12]

Figure 4.3, above, shows that there are two semicircles in the Nyquist plot. This means that the system has two time constants, one for the cathode side and another for the anode side. The diameters of the semicircles represent the resistance of that part of the cell. Because of the much faster kinetics at the anode, the resistance has a larger value there, than at the cathode. Usually, the smaller semicircle is too small to be visualized and in many cases removed to make the system simpler to analyze. The later section of the graph is linear, and is represented by the Warburg element. [12]

Software used for EIS analysis today usually contains a lot of different circuit models to describe the electrochemical processes. The above mentioned models are the most basic ones, the ones that are closest to the most common electrical components.

5 THE EXPERIMENTAL DEVICE

In this thesis for the EIS measurements an experimental device was used. The device is shown in Figure 5.1. For measuring, this unit is connected to a computer via USB cable and is controlled by software. Through this software the unit is run by typing in commands into command line.

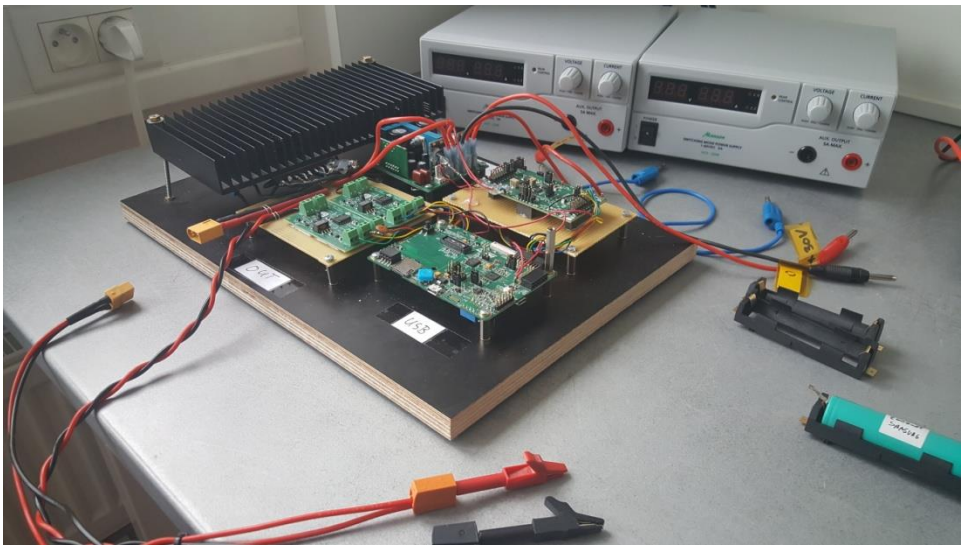

Figure 5.1 Experimental device

The available commands and changeable variables are included in Table 5.1 and Table 5.2 respectively.

Table 5.1 Commands

Commands	
status	displays live status
config	displays configuration
reset	resets system
upgrade	starts firmware updater
enable	enables power output
disable	disables power output
get	returns current measurement results
sweep	starts a frequency sweep
stop	aborts a running sweep
poll	returns available data from running sweep

To display the value of the variable, typing in the name is enough. Changing the value of a variable is also simple; it has to be written as an equation. For example: sftart=10.0 would set the start frequency to 10.0 Hz.

Table 5.2 Variables

Variables	
serial	shows system serial number (read only)
date	shows firmware creation date (read only)
average	sets number of periods to average
skip	sets number of periods to skip before averaging (sweep mode)
time	sets sweep minimum measurement time per sample (sweep mode, seconds)
mode	configures operation mode: 0 = GEIS, 1 = PEIS
vmin	sets minimum output voltage (Volts)
vmax	sets maximum output voltage (Volts)
imin	sets minimum output current (Amperes-PEIS AC amplitude only)
imax	sets maximum output current (Amperes-PEIS AC amplitude only)
ampl	sets instantaneous AC amplitude (GEIS: Amperes, PEIS: Volts)
dc	sets instantaneous DC current level (Amperes)
f	sets instantaneous AC frequency (Hertz)
sampl	sets sweep AC amplitude (GEIS: Amperes, PEIS: Volts)
sdc	sets sweep DC current level (Amperes)
sfstart	sets sweep starting frequency (Hertz)
sfend	sets sweep final frequency (Hertz)
step	sets sweep frequency step (positive: lin step in Hertz, negative: log multiplier)

This device uses the four-terminal sensing method as an electrical impedance measuring method. Separate pairs of current-carrying and voltage-sensing electrodes are used. This gives more accurate measurements. Separation of current and voltage electrodes reduce the lead and contact resistance from the measurement.

Some additional technical information: the maximum DC discharge current is 3 A, the maximum DC charge current is 2 A and the maximum AC test current is 5V. The unit operates only on single cell batteries and only up to 5 Volts. There is no over-temperature protection.

For safe operation, it is important to connect and disconnect the batteries only when the output is disabled. First the command “disable” has to be typed in, then the battery is connected and following the “enable” command is used. The selection between the two different types of measuring methods is done with the “mode” variable. Setting it to 0 will enable the galvanostatic method, 1 the potentiostatic method. The unit has two modes of operation: not sweeping or sweeping. The “sweep” command starts the AC impedance measurements at different frequencies. The sweep parameters are given by the variables: “sampl”, “sdc”, “sfstart”, “sfend”, “step”, “average” and “skip”. After the correct setup the battery can be connected and a sweep can be started. During the sweep the available data is shown by typing in “poll”. This command will write out all the measured data in a row like this: number of the

measured data, frequency, voltage (AC amplitude), voltage (DC component), current (AC amplitude), current (DC component), phase (between the AC voltage and current). Everything that is typed into the command line is also saved into a text document.

5.1 Parts of the device

The device uses symmetrical supply of power (± 30 V) and can only be used for one cell batteries. This supply of ± 30 V is needed to operate the power amplifier part of the device. The power amplifier shown on Figure 5.2 is responsible for creating the measuring signals (sinusoid signal, for GEIS a current signal, for PEIS a voltage signal).

Figure 5.2 The power amplifier

A digital to analog converter (DAC) is used with the power amplifier. The device is from Texas Instruments and uses the DAC8801 multiplying digital-to-analog converter. This part of the device is in Figure 5.3. The applied external reference input voltage V_{REF} determines the full-scale output current, when combined with an external I-to-U precision amplifier an internal feedback resistor (R_{FB}) provides temperature tracking. [13]

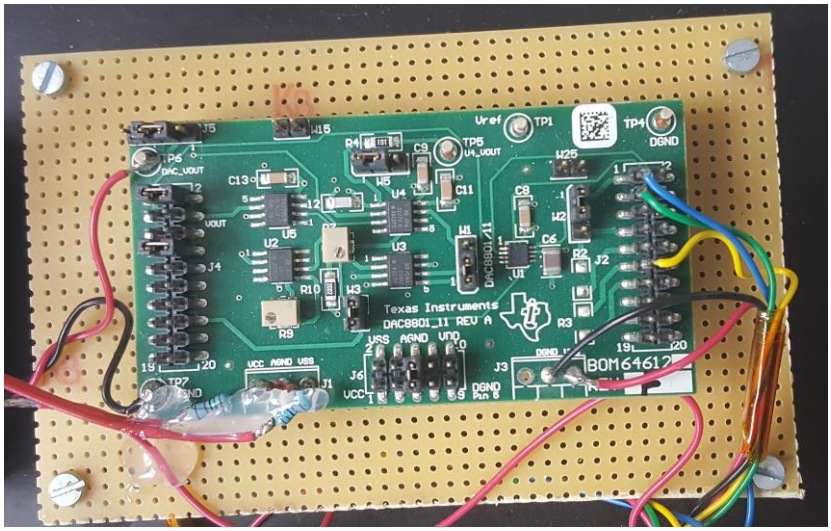

Figure 5.3 DAC for power amplifier

For measuring the AC voltage and current an analog digital converter (ADC) is used. Shown in Figure 5.4 is the module used in the device, it consist of two AMC1305EVM modules from Texas Instruments. The AMC1305 device is a precision, delta-sigma (ΔΣ) modulator that separates the output from the input circuitry by a capacitive double isolation barrier. This barrier is highly resistant to magnetic interference. The AMC1305 is optimized for direct connection to shunt resistors or other low voltage level signal sources supporting excellent dc and ac performance. [14]

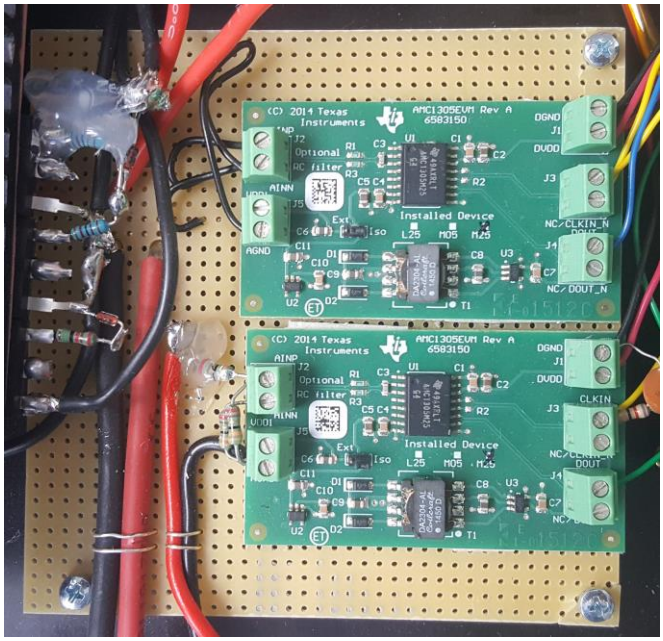

Figure 5.4 Voltage and current measurement ADC's

Controlling the experimental device is done with a microcontroller module from STMicroelectronics. The module used in the device is 32L4R9IDISCOVERY kit and it's shown in Figure 5.5. This module is a complete demonstration and development platform based on the STM32L4R9AI microcontroller, a user-friendly unit that provides out-of-the-box programming and debugging capabilities. [15]

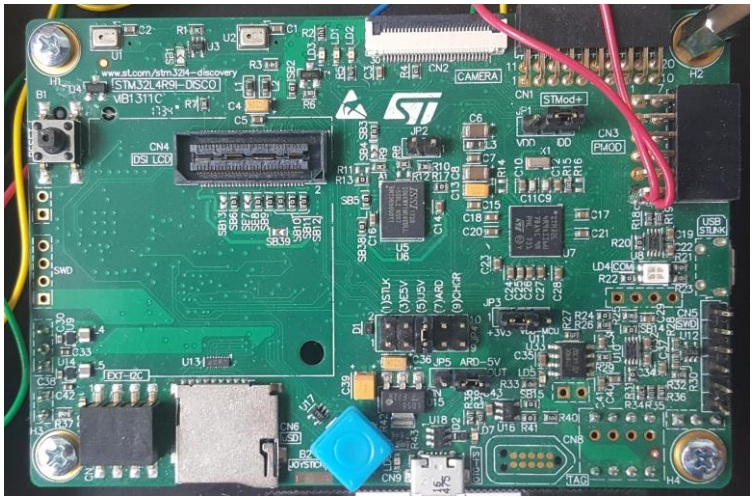

Figure 5.5 Microcontroller unit

6 RESULTS OF THE MEASUREMENTS

The measurements were conducted with the VMP-300 device from BioLogic Science Instruments. These measurements were used as reference data for the comparison. The two methods of measurement were the galvanostatic electrochemical impedance spectroscopy (GEIS) and the potentiostatic electrochemical impedance spectroscopy (PEIS). The same measurements were done with the experimental device. Microsoft Excel was used to process the data and graphs were generated.

The setup for the measurements were kept as close to each other as possible between the two devices. With GEIS the measuring signal was a sinusoid current with an amplitude of 1 A. The reason for such high amplitude was the experimental device; smaller amplitudes produced only a noise signal. In the case of PEIS the signal was a sinusoid voltage with amplitude of 100 mV (higher values to reduce the noise in the signal). The frequency range was set from 50 kHz to 50 mHz, measuring six data points in every decade. With the device from BioLogic this was a straight setup parameter: N_d=6 points/decade in logarithmic spacing, and with the experimental device the variable step was set to -1,468 (as described in Chapter 5, Table 5.2). The rest of the setup consists of the voltage and current limits for the measurements and the value of averaging. Average N_a=3 measure(s)/frequency (the BioLogic device) and the average with the experimental device was set to 30 (as described in Chapter 5, Table 5.2). The reason for a ten times higher averaging count was to get more accurate measurements from the experimental device (signal noise with lower values of averaging was prevalent).

The measurements were carried out on two types of batteries, Panasonic NCR 18650 B and NCR 18650 F. Two of each types were measured. Furthermore the batteries were measured in fully charged states (based on the values in the datasheet, they were charged to 4,1 V) and in discharged states (they were not fully discharged, in the datasheet the lower limit is 2,5 V, they were discharged to 2,8 V). On the experimental device the connection leads were first used with crocodile clips (connected to the contacts of the battery holder), and then they were soldered to the battery holder, in order to reduce the added impedance of the measuring wires and connections.

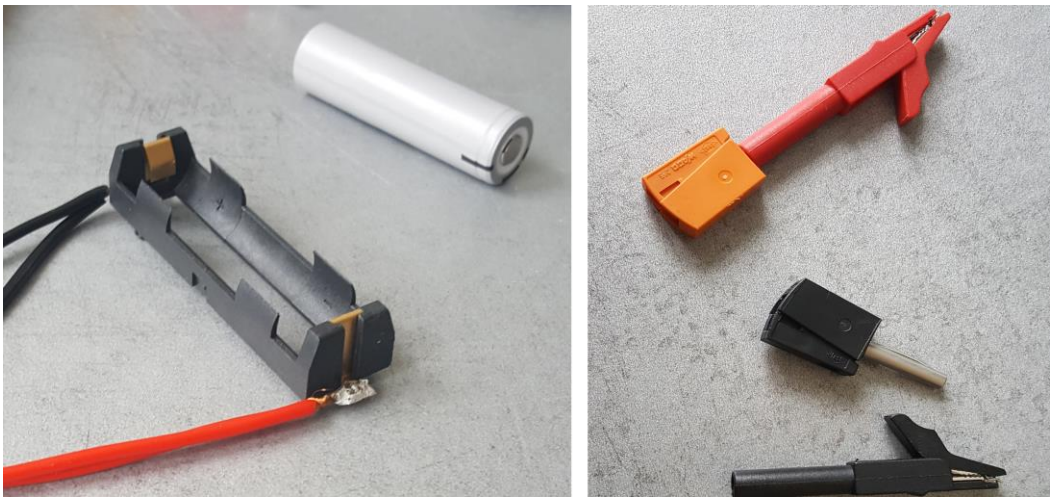

Figure 6.1 a.) The wires soldered to the battery holder, b.) The crocodile clips used for connecting the wires to the battery holder

6.1 Interpretation of the data

For this analysis the results from the experimental device were used. These results are for the NCR 18650 B type battery after soldering the contacts to the battery holder. Figure 6.2 shows the result in a Nyquist Plot.

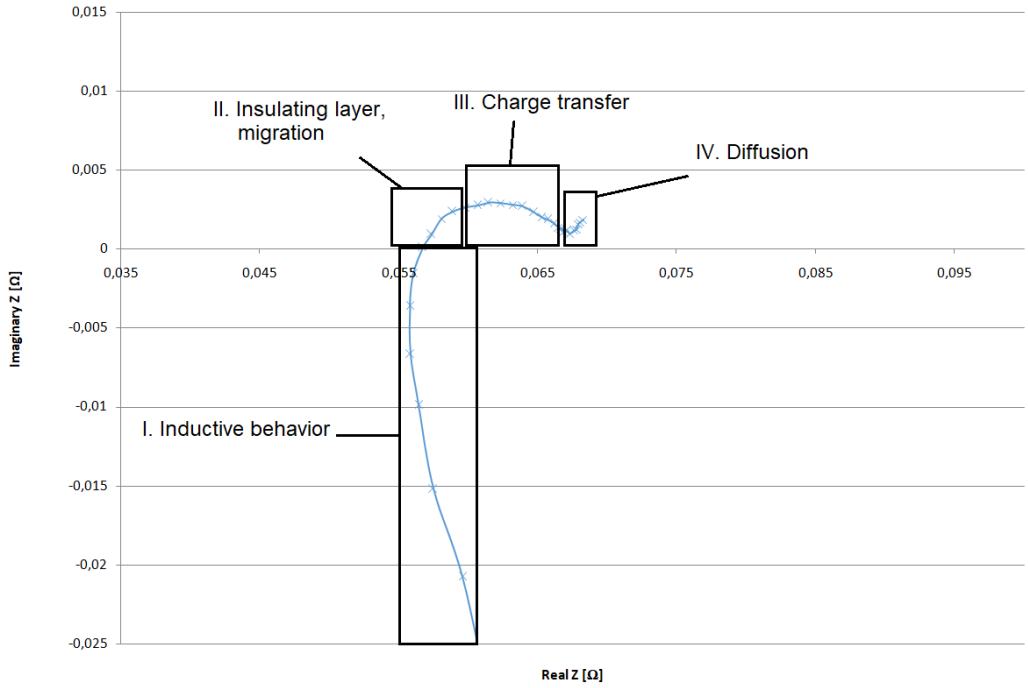

Figure 6.2 Panasonic NCR 18650 B in charged state (zoomed in)

I. The highest frequencies show an inductive behavior. Usually this part represents the inductive properties of the measuring wires and/or the battery electrode itself. The intersection with the x-axis represents the total Ohmic resistance of the system. This includes the electrolyte resistance and the contact resistance.

II. This part represents the interlayer effects at the solid electrolyte interface, the passing through of charges. It describes the de- or intercalation of the Lithium ions into the active material. The solid state diffusion of Lithium ions is compelled by the concentration gradient of ions between the surface and the bulk of the electrode.

III. The curve at mid-range frequencies (kHz to Hz range) corresponds to the charge transfer kinetics. It designates the electrons conduction from one electrode to the other and the conduction through the outside circuit.

IV. The arc at very low frequencies (near DC) is associated with the diffusion behavior. This means the ions conduction in the electrolyte through the separator, which is forced by the concentration gradient and it happens at a higher rate than in solids.

These processes can be described by equivalent circuit modeling of the impedance response (described in Chapter 4). Some of the more common types of elements include: C_{dl}-the electrochemical double layer capacitance, R_{CT}-the faradaic charge transfer resistance, C_{int}-the intercalation capacitance corresponding to the accumulation of the lithium ions, $Z(\omega)$-the Warburg solid-state impedance. [16]

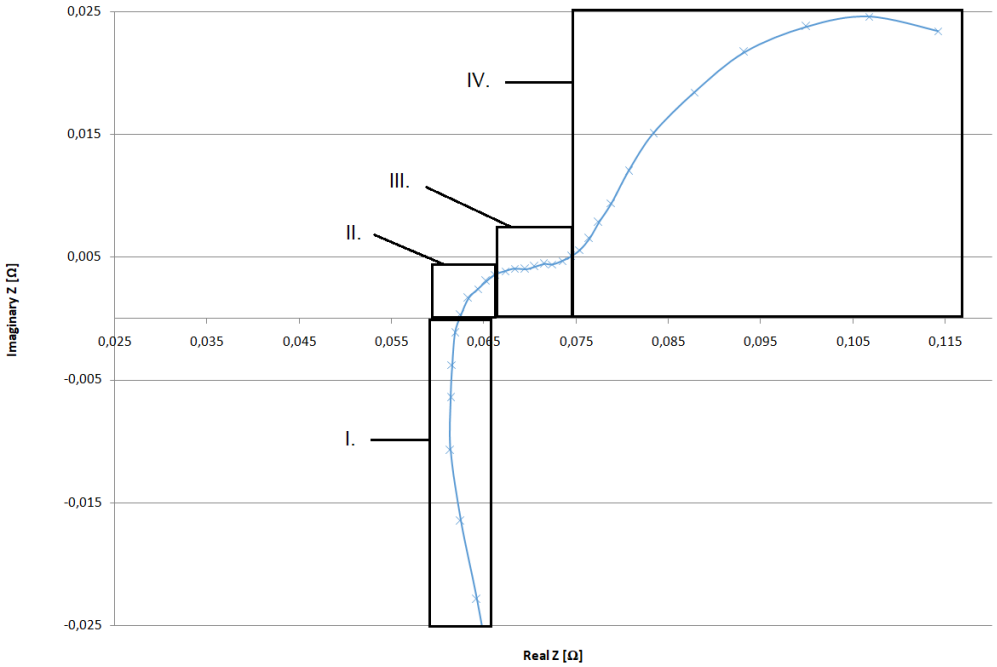

Figure 6.3 Panasonic NCR 18650 B in discharged state (zoomed in)

The difference between a charged and discharged Nyquist Plot are instantly visible. However the first two areas in the graph are similar. These chemical processes are almost identical; the difference is due to the state of charge (SOC). However the SOC doesn't seem to have a huge impact on the Ohmic resistance at the intersection with the x-axis. The differences lie in the charge transfer rate (area III.), where the internal resistance increases. This can be interpreted as an effect of the low SOC state, the electrode is close to full discharge, and no obvious electrode reaction occurs, resulting in increased charge transfer impedance. In the fourth part of the graph the diffusion impedance is affected. The shape of the Nyquist Plot and the increased values of the diffusion impedance are due to the empty state of the electrode at the end of the discharge phase, making it more difficult for Li+ to embed or detach from the active material. [17]

With discharged batteries the Nyquist Plot curves were consistent, part of the high frequency curve is concentrated, while the low and medium frequency curve is relatively dispersed. Even between the two methods (PEIS and GEIS) were no significant differences. What differed was usually the Ohmic resistance at the intersection with the x-axis. These differences can be caused by the charge and discharge processes, was it properly charged (discharged), how long was it charged (discharged) and how long was the battery not used between charging and discharging cycles. [17]

6.2 Comparison between PEIS and GEIS

For this part the results of EIS on the Panasonic NCR 18650 F type were used. The Bode Plot with the real and imaginary parts of the impedance is shown on Figure 6.4. These were measured on the same Panasonic NCR 18650 F battery.

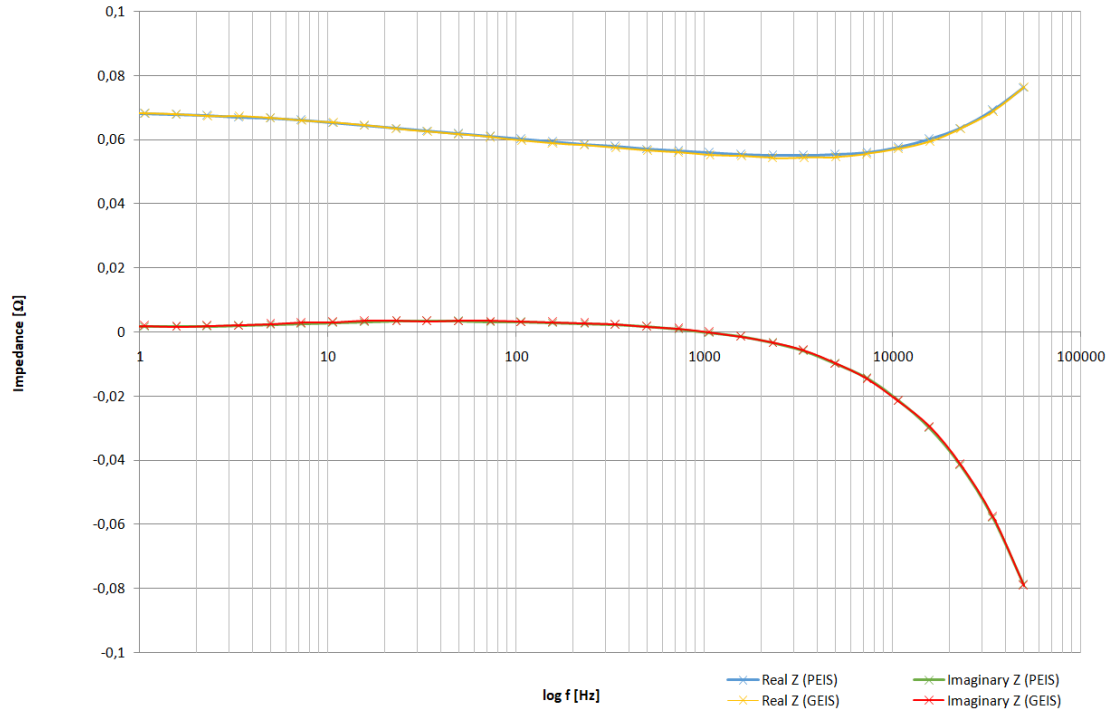

Figure 6.4 Panasonic NCR 18650 F in charged state, PEIS and GEIS (impedance plot)

As the Figure 6.4 shows the difference between the methods is negligible, with the naked eyes non-visible. Similarly the results of EIS on the Panasonic NCR 18650 F in a discharged state are also minimal, barely visible, shown in Figure 6.5.

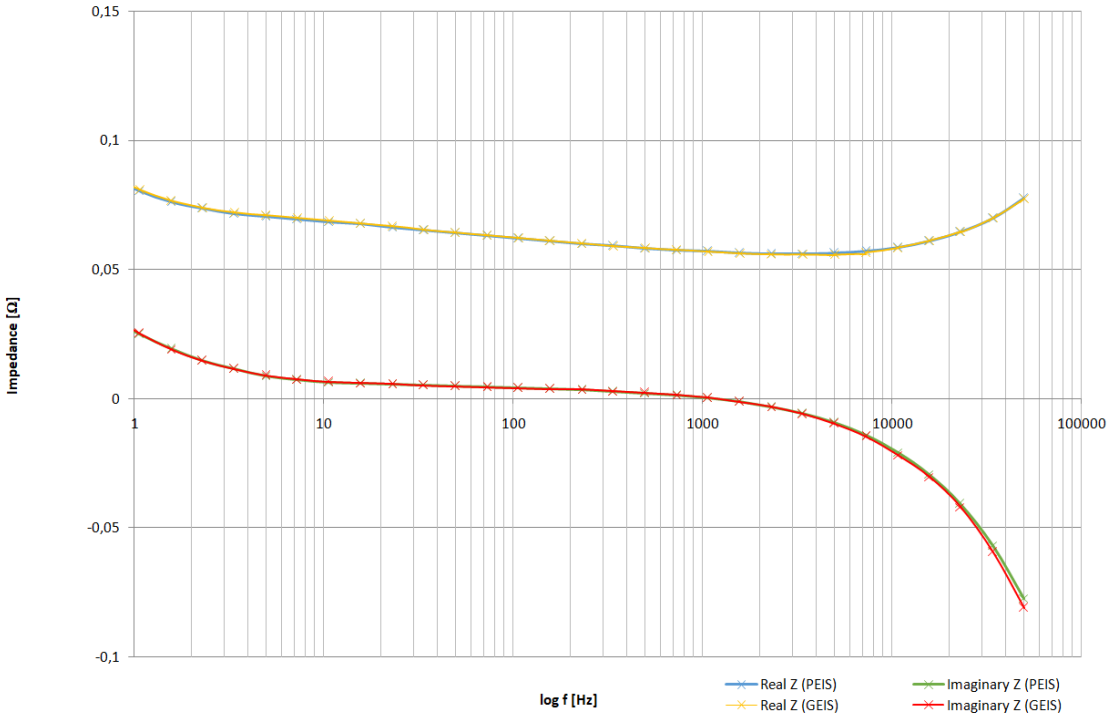

Figure 6.5 Panasonic NCR 18650 F in discharged state, PEIS and GEIS (impedance plot)

Figure 6.6 and 6.7 shows the Bode Plot with the phase, measured on the same Panasonic NCR 18650 F battery.

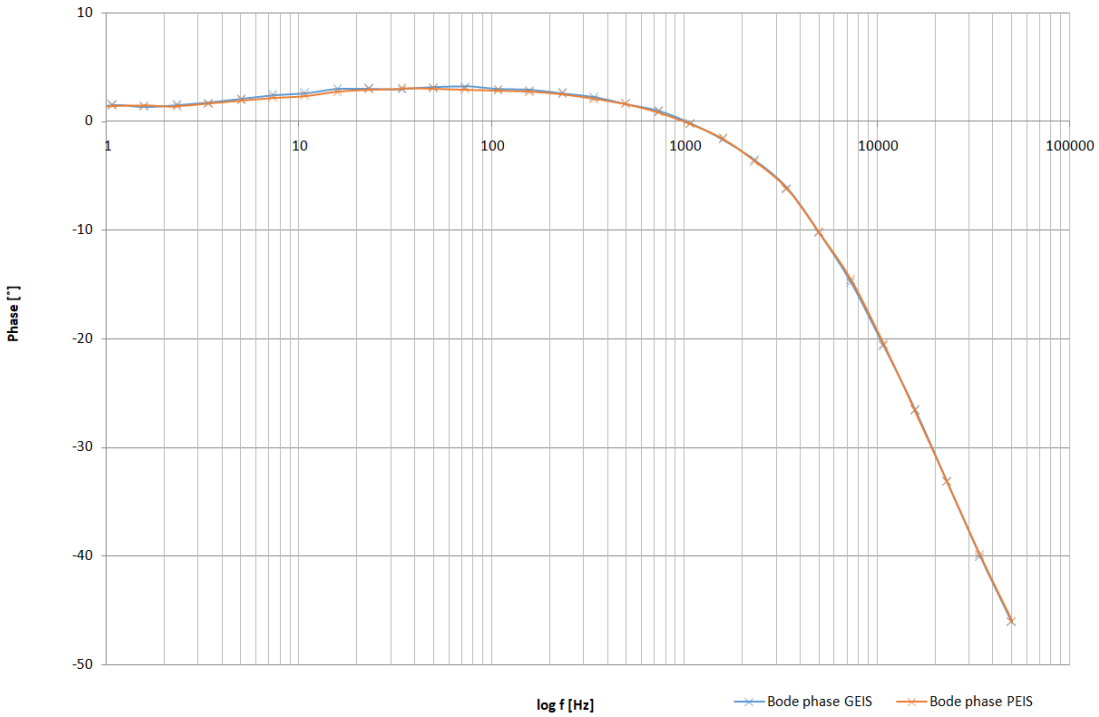

Figure 6.6 Panasonic NCR 18650 F in charged state, PEIS and GEIS (phase plot)

Similarly the results shown in a Bode Plot with phase are also negligible.

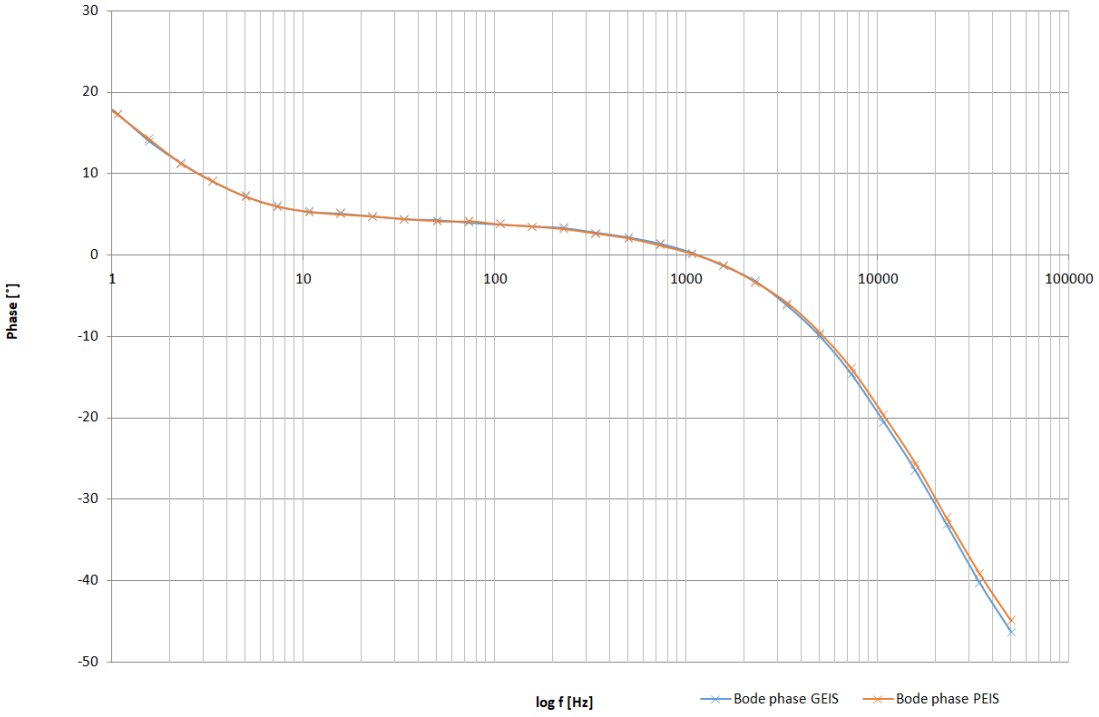

Figure 6.7 Panasonic NCR 18650 F in discharged state, PEIS and GEIS (phase plot)

6.3 Comparison between the experimental device and the BioLogic device

In this part the results of EIS measurements with the experimental and BioLogic devices are shown. The results of PEIS and GEIS measurements are compared for both types of battery, separately. As before, the measurements were done on fully charged batteries and discharged batteries. The comparison with the GEIS method is shown in Figure 6.8.

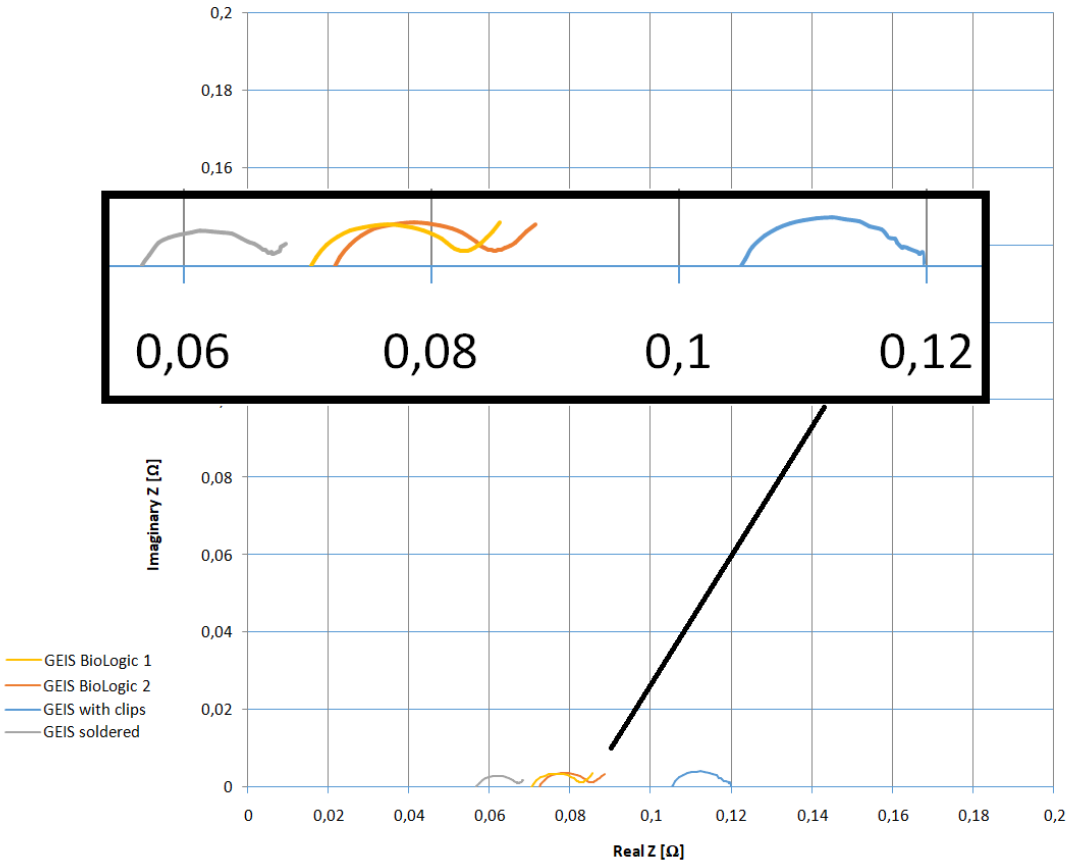

Figure 6.8 Panasonic NCR 18650 B in charged state, GEIS

There are two reference curves (GEIS BioLogic 1, GEIS BioLogic 2) on the graph, the reason being, that the measurements with the experimental device were carried out at different times, so individual reference measurements were made. Between the two measurements the batteries were discharged and charged multiple times. Even after that, the reference values are very close to each other.

Table 6.1 The Ohmic resistance of the GEIS (Panasonic NCR 18650 B, charged)

Name of the curve	R [Ω]
GEIS BioLogic 1	0,072
GEIS BioLogic 2	0,071
GEIS with clips	0,105
GEIS soldered	0,057

Table 6.1 highlights the Ohmic resistances at the intersection with the x-axis. This shows the affect of the type of connection used with the experimental device. Soldering the contacts significantly reduced the resistance.

The reference curve GEIS BioLogic 2 is corresponding to the curve measured with the experimental device after soldering the contacts to the battery holder (GEIS soldered). The other curve (GEIS BioLogic 1) is the reference for the curve GEIS with clips.

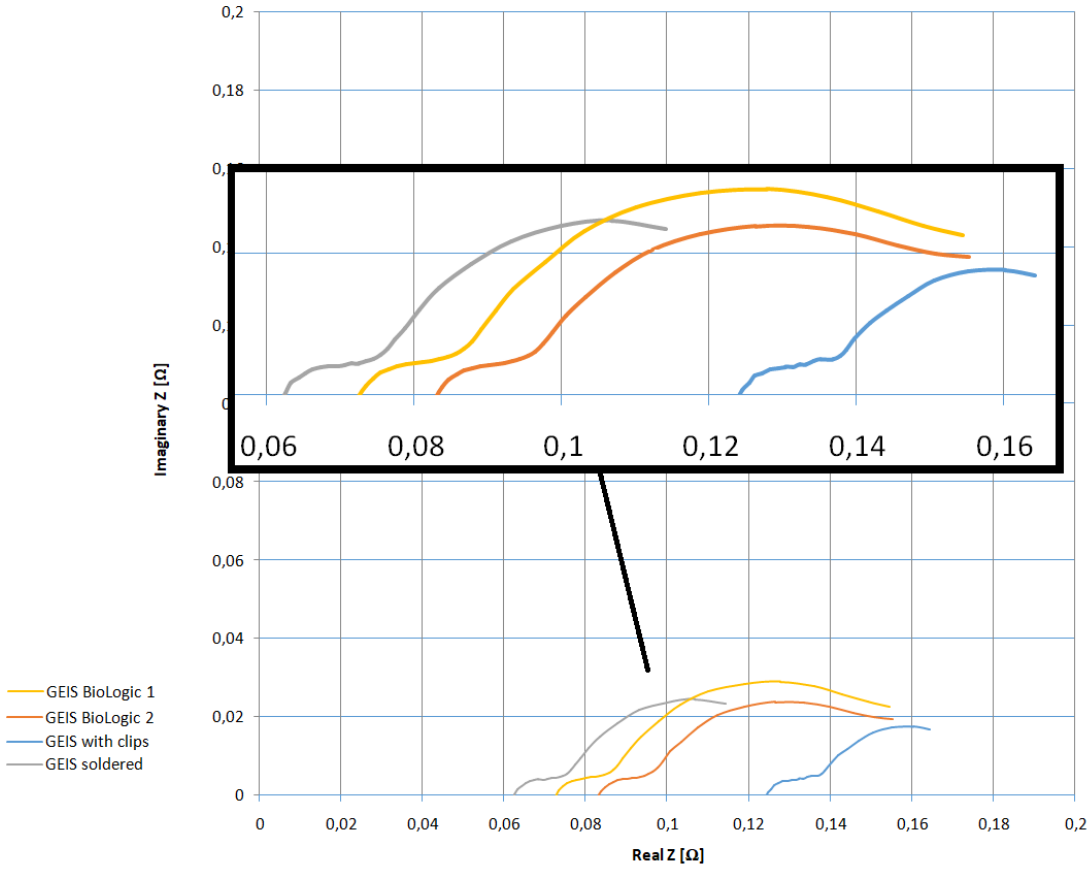

Figure 6.9 Panasonic NCR 18650 B in discharged state, GEIS

Figure 6.9 shows the comparison between the results of the measurements on a discharged Panasonic NCR 18650 B type battery.

Table 6.2 The Ohmic resistance of the GEIS (Panasonic NCR 18650 B, discharged)

Name of the curve	R [Ω]
GEIS BioLogic 1	0,083
GEIS BioLogic 2	0,073
GEIS with clips	0,124
GEIS soldered	0,062

The affect of soldering the contacts is shown in Table 6.2. For the discharged battery the resistance also decreases.

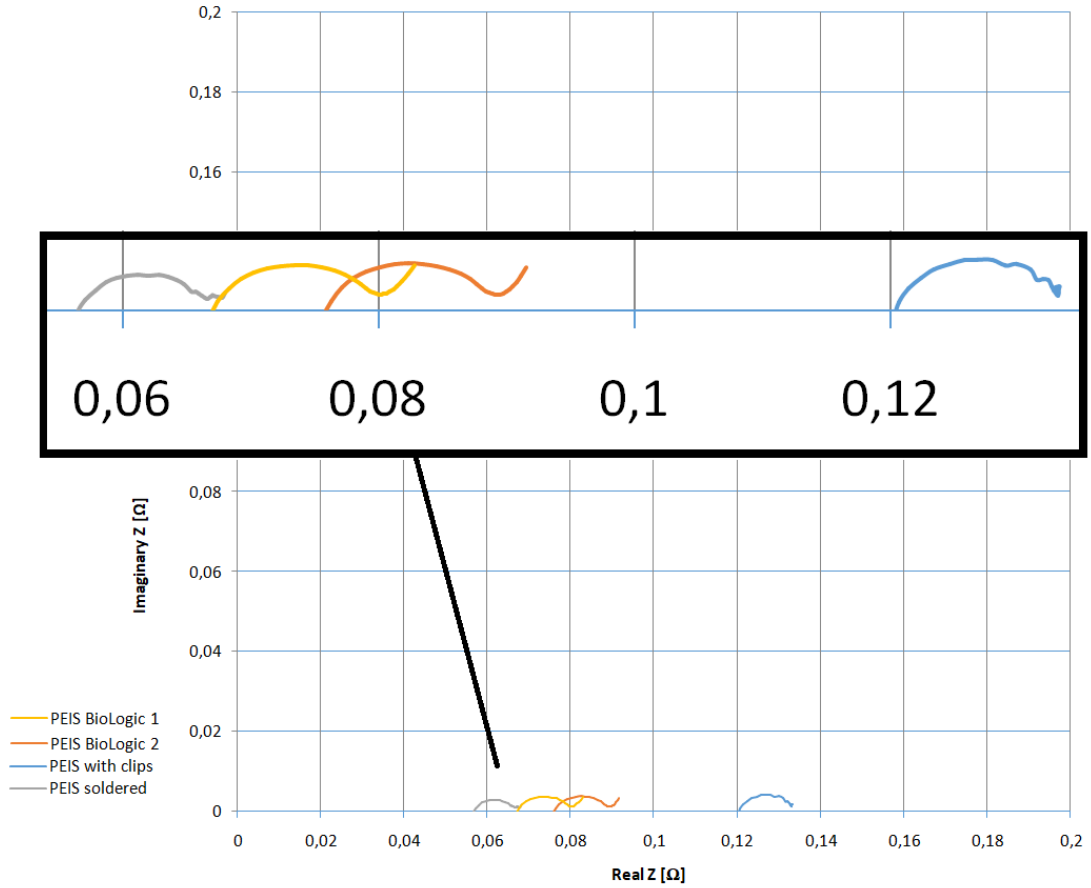

Figure 6.10 Panasonic NCR 18650 B in charged state, PEIS

Figure 6.10 compares the results measured on a fully charged Panasonic NCR 18650 B type battery.

Table 6.3 The Ohmic resistance of the PEIS (Panasonic NCR 18650 B, charged)

Name of the curve	R [Ω]
PEIS BioLogic 1	0,076
PEIS BioLogic 2	0,067
PEIS with clips	0,121
PEIS soldered	0,057

The affect of soldering the contacts shows the same trend with PEIS method as well. The resistance values are shown in Table 6.3.

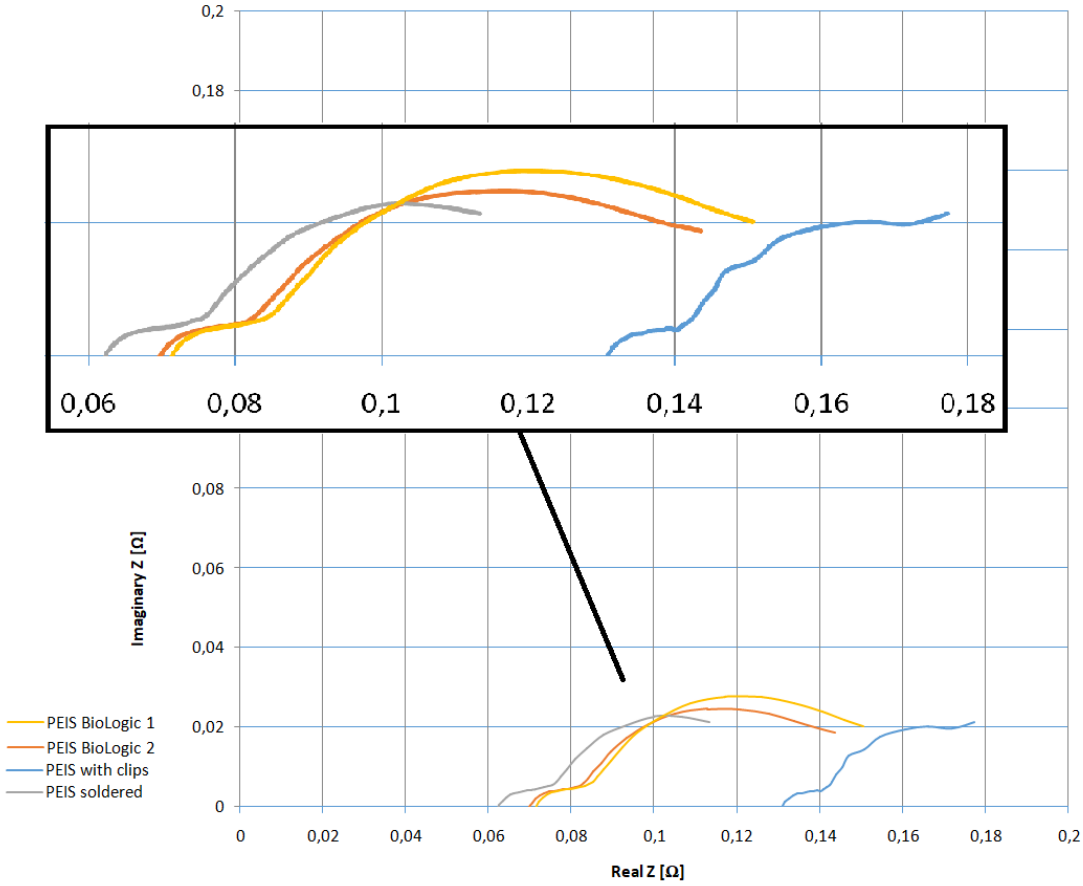

Figure 6.11 Panasonic NCR 18650 B in discharged state, PEIS

Figure 6.11 compares the results of the measurements on a discharged Panasonic NCR 18650 B type battery.

Table 6.4 The Ohmic resistance of the PEIS (Panasonic NCR 18650 B, discharged)

Name of the curve	R [Ω]
PEIS BioLogic 1	0,070
PEIS BioLogic 2	0,071
PEIS with clips	0,131
PEIS soldered	0,062

The resistance values are shown in Table 6.4. The same as before the resistance is reduced by bypassing the crocodile clips.

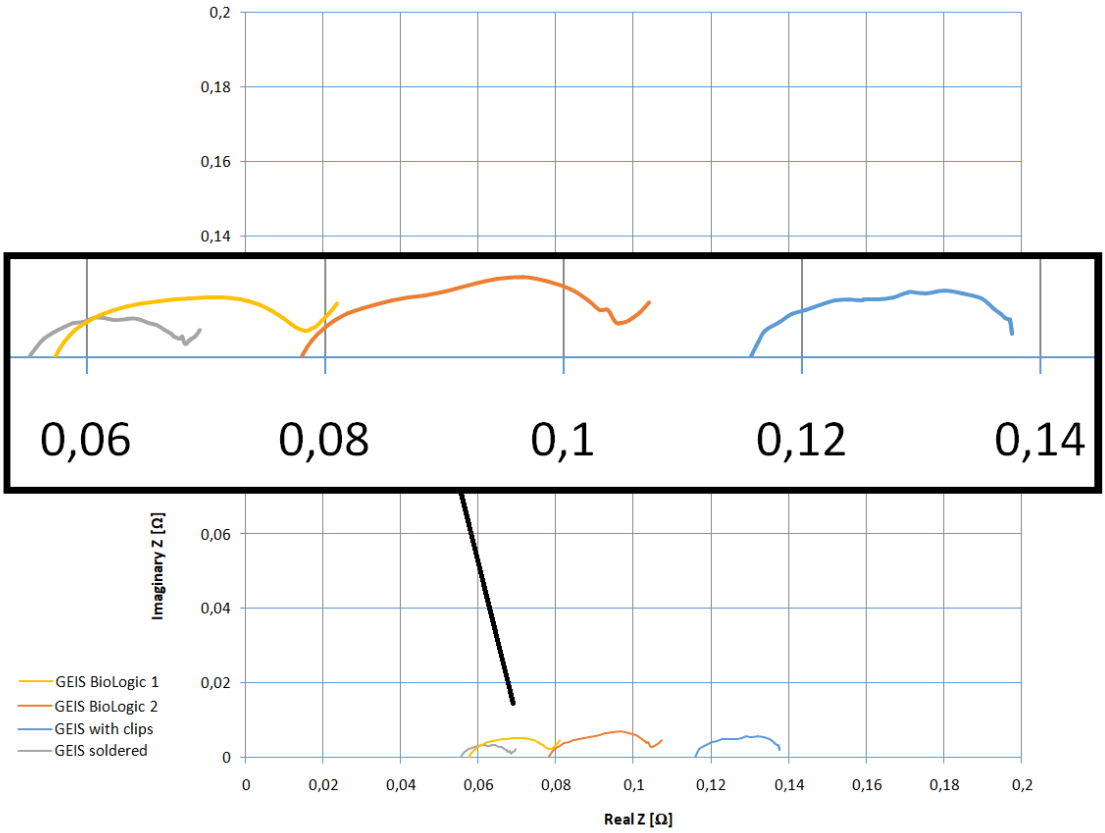

Figure 6.12 Panasonic NCR 18650 F in charged state, GEIS

Figure 6.12 shows the results with a fully charged Panasonic NCR 18650 F type battery.

Table 6.5 The Ohmic resistance of the PEIS (Panasonic NCR 18650 F, charged)

Name of the curve	R [Ω]
GEIS BioLogic 1	0,078
GEIS BioLogic 2	0,057
GEIS with clips	0,116
GEIS soldered	0,055

The resistance values are shown in Table 6.5. The same as before the resistance is reduced by bypassing the crocodile clips. With the Panasonic NCR 18650 F battery the reference values differ as well. This is can be due to the discharge process itself or the amount of time the battery was idle. It is, however closer to the curve measured with the experimental device.

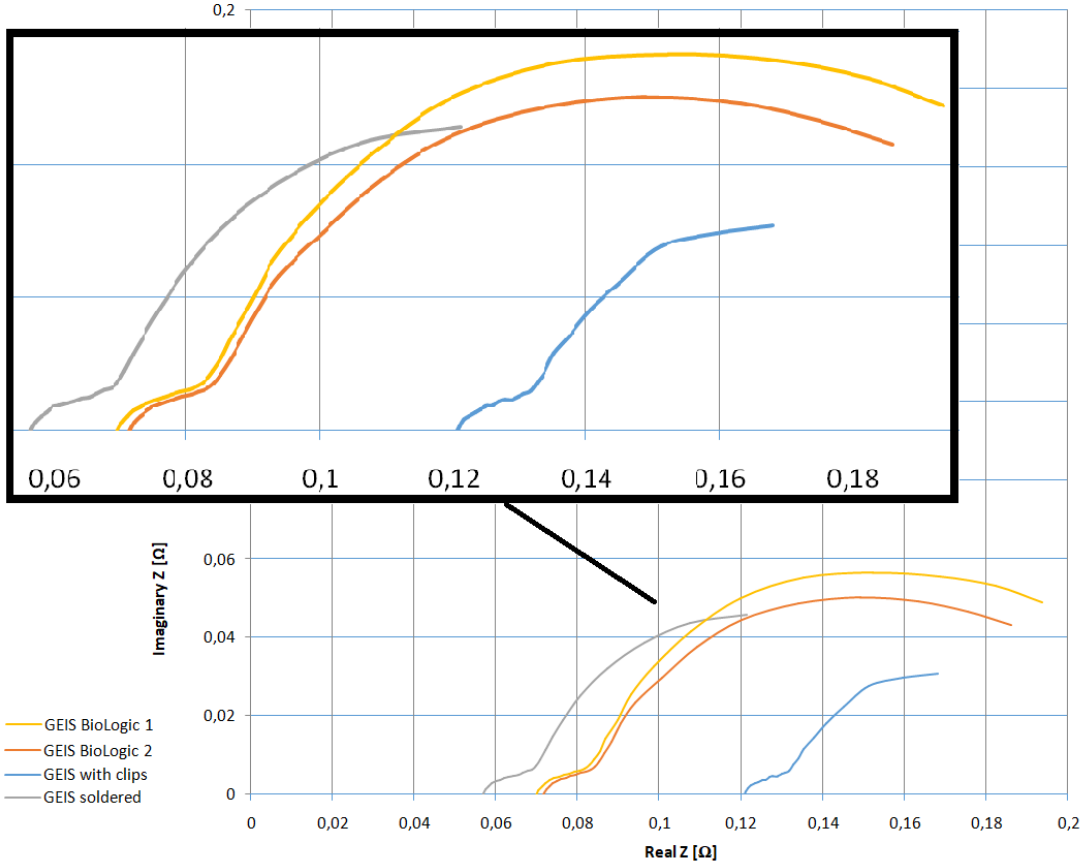

Figure 6.13 Panasonic NCR 18650 F in discharged state, GEIS

Figure 6.13 shows the results with a discharged Panasonic NCR 18650 F type battery.

Table 6.6 The Ohmic resistance of the PEIS (Panasonic NCR 18650 F, discharged)

Name of the curve	R [Ω]
GEIS BioLogic 1	0,071
GEIS BioLogic 2	0,070
GEIS with clips	0,121
GEIS soldered	0,057

The resistance values are shown in Table 6.6. The same as before the resistance decreases after soldering the wires to the battery holder. This time the reference values are nearly identical, showing the importance of the discharging process.

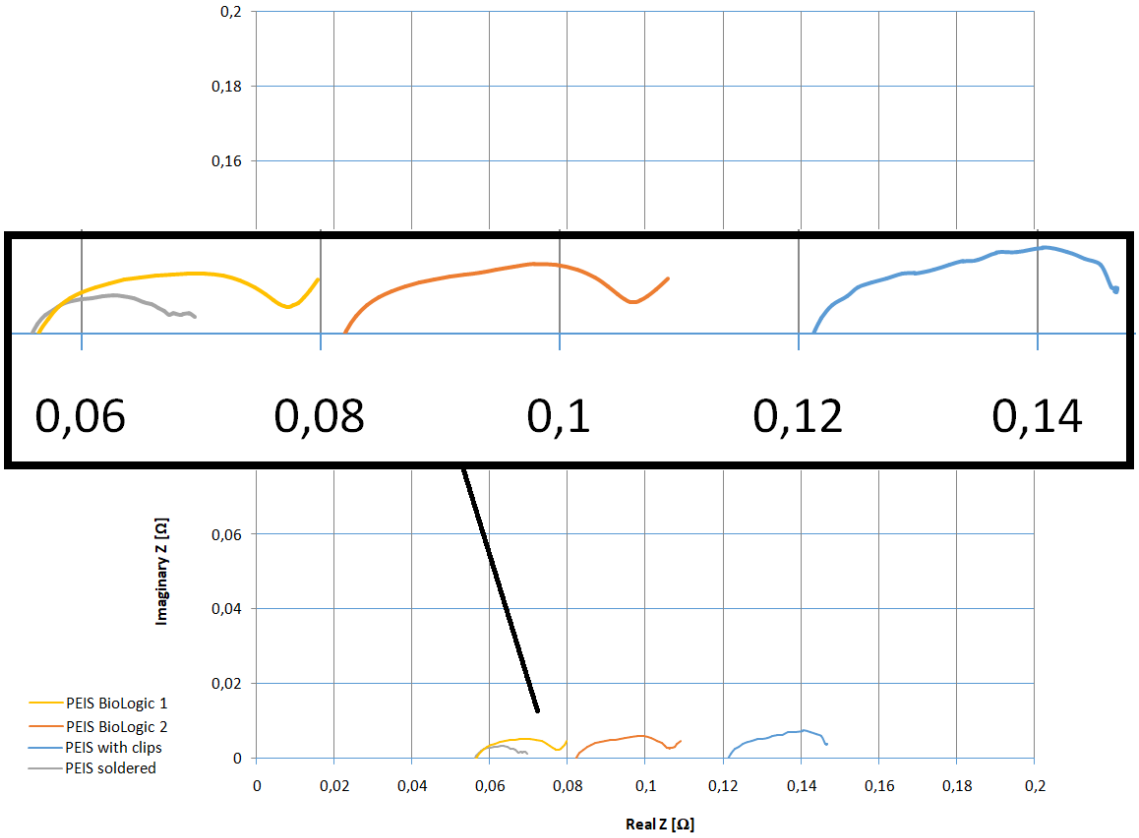

Figure 6.14 Panasonic NCR 18650 F in charged state, PEIS

Figure 6.14 shows the results of measuring with the PEIS method on a fully charged Panasonic NCR 18650 F type battery.

Table 6.7 The Ohmic resistance of the PEIS (Panasonic NCR 18650 F, charged)

Name of the curve	R [Ω]
PEIS BioLogic 1	0,082
PEIS BioLogic 2	0,056
PEIS with clips	0,120
PEIS soldered	0,056

The resistance values are shown in Table 6.7. The same as before the resistance is reduced after soldering the wires to the battery holder. Like with the GEIS method the reference values differ, however this time, the measurement after soldering and the corresponding reference values have the same Ohmic resistance.

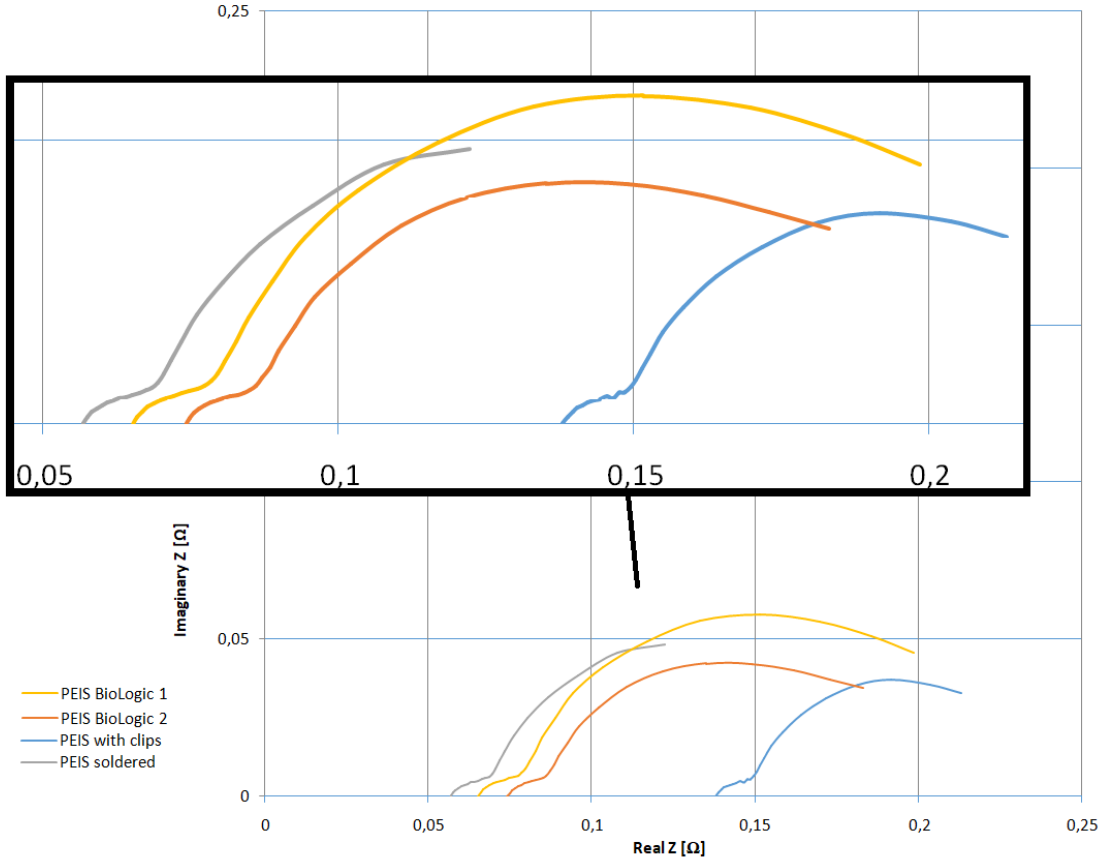

Figure 6.15 Panasonic NCR 18650 F in discharged state, PEIS

Figure 6.15 shows the results of measuring with the PEIS method on a discharged Panasonic NCR 18650 F type battery.

Table 6.8 The Ohmic resistance of the PEIS (Panasonic NCR 18650 F, discharged)

Name of the curve	R [Ω]
PEIS BioLogic 1	0,074
PEIS BioLogic 2	0,065
PEIS with clips	0,138
PEIS soldered	0,057

Table 6.8 shows the resistance values. The same as before the resistance is reduced by bypassing the crocodile clips. Out of all the measured values these are the closest to each other. The biggest difference was measured, when the crocodile clips were used to connect the battery.

The visible trend with these comparisons was that, reducing the resistance of the connection with the experimental device (by directly soldering it to the battery holder) got the values closer to the reference data. This shows that the experimental device needs further calibration, but is capable of producing reliable data.

6.4 Summary

To summarize the results a table containing the last values of the Ohmic resistance of the measurements was created.

Table 6.9 The Ohmic resistance of the measurements

Type of battery	Name of the curve	R [Ω]	Δ_R [Ω]	δ_R [%]
Panasonic NCR 18650 B charged state	**GEIS with clips**	0,105		
	GEIS BioLogic 1	0,072	0,033	31,429
	GEIS soldered	0,057		
	GEIS BioLogic 2	0,071	-0,014	-24,561
Panasonic NCR 18650 B discharged state	**GEIS with clips**	0,124		
	GEIS BioLogic 1	0,083	0,041	33,065
	GEIS soldered	0,062		
	GEIS BioLogic 2	0,073	-0,011	-17,742
Panasonic NCR 18650 B charged state	**PEIS with clips**	0,121		
	PEIS BioLogic 1	0,076	0,045	37,190
	PEIS soldered	0,057		
	PEIS BioLogic 2	0,067	-0,01	-17,544
Panasonic NCR 18650 B discharged state	**PEIS with clips**	0,131		
	PEIS BioLogic 1	0,070	0,061	46,565
	PEIS soldered	0,062		
	PEIS BioLogic 2	0,071	-0,009	-14,516
Panasonic NCR 18650 F charged state	**GEIS with clips**	0,116		
	GEIS BioLogic 1	0,078	0,038	32,759
	GEIS soldered	0,055		
	GEIS BioLogic 2	0,057	-0,002	-3,636
Panasonic NCR 18650 F discharged state	**GEIS with clips**	0,121		
	GEIS BioLogic 1	0,071	0,05	41,322
	GEIS soldered	0,057		
	GEIS BioLogic 2	0,070	-0,013	-22,807
Panasonic NCR 18650 F charged state	**PEIS with clips**	0,120		
	PEIS BioLogic 1	0,082	0,038	31,667
	PEIS soldered	0,056		
	PEIS BioLogic 2	0,056	0	0,000
Panasonic NCR 18650 F discharged state	**PEIS with clips**	0,138		
	PEIS BioLogic 1	0,074	0,064	46,377
	PEIS soldered	0,057		
	PEIS BioLogic 2	0,065	-0,008	-14,035

Figures 6.8 to 6.15 show the results from the different battery types and states of charge, corresponding to Table 6.9. On these figures the shape of the curves is visible (for better visibility it is zoomed in). The constructed table compares the Ohmic resistance of the measurements, which shows the affect of the added impedance to the measuring wires. In order to get more accurate results (compared to the reference values from the BioLogic instrument), the measuring wires were soldered to the battery holder. This reduced the unwanted, added resistance and got the values closer to the reference measurements. Table 6.9 also shows the absolute and relative deviation. The differences clearly show how much the results improved bypassing the resistance of the crocodile clips. The deviations Δ_R (in Ω) and δ_R (in %) were calculated with the following equations:

$$\Delta_R = X_M - X_{REF}, \tag{6.1}$$

$$\delta_R = \frac{\Delta_R}{X_M}.100, \tag{6.2}$$

where X_M is the data measured with the experimental device and X_{REF} is the reference data (measured with the BioLogic instrument).

On the mentioned figures the shape of the Nyquist Plot is also visible, where the differences in the curves are due to the affect of the charging and discharging processes. Leaving the battery to charge longer affects the "length" of the semi-circle (the impedance of the battery), which can mean over-charging or under-charging (if not charged for the proper time). The results are also affected by the measuring signals, higher current and voltage amplitudes can also be the cause of the differences between the two devices. After getting closer to the reference values, additional measurements could be conducted to determine the optimal amplitudes for the measuring signals. The higher values, 1 A for GEIS and 100 mV for PEIS, were used because of the experimental device. The device needed these values in order to measure correctly. Lower values yielded poor results; only the signal noise was measured. The BioLogic instrument usually measures with lower values, for PEIS 10 mV is commonly used and for GEIS even couple mili-amperes (even micro-amperes) can be used.

Chapter six also contains a comparison between the measuring methods (PEIS, GEIS), shown on Figures 6.4 and 6.5, for charged and discharged states, respectively. For this comparison the Bode Plot of the complex impedance was used, measured with the experimental device. The plot contains both the real and imaginary part of the impedance and shows no visible differences between the methods of measurement. The curves in the plot completely overlay. The Bode Plots with phase shift are also included, Figure 6.6 and 6.7.

The results of these measurements show, that the experimental device is a viable tool for measuring EIS. The differences are not significant and with more measurements and experiments it could produce the exact same results as a commercially available instrument.

7 CONCLUSION

This diploma thesis focuses on attaining the information needed to understand the working principal of the lithium-ion batteries. Furthermore the electrochemical impedance spectroscopy methods are described. This description contains the difference between the galvanostatic and potentiostatic method, the mathematical models of how to process the acquired data and the information on how to operate the experimental device. The first step was to study through the above described information about lithium-ion batteries and the electrochemical spectroscopy method. Secondly a proper workstation had to be set up. A computer alongside with two power supplies was needed to start up the experimental device. This device uses symmetrical supply of power (± 30 V) and can only be used for one cell batteries.

After setting up the workstation and getting familiar with how the experimental device functions the first task was to get the device up and running. The variables and commands described in chapter five are used to operate the device. It can use both the galvanostatic and potentiostatic electrochemical impedance methods. The measuring signal is a sinusoid signal with amplitude set by the variable sampl (for both methods). Selecting the measuring method is done with the mode variable (mode=0 for GEIS and mode=1 for PEIS). The other variables are used to set the measuring parameters. The frequency range is set by the variables sfstart and sfend. The variables average, step, skip describe the number of measurements on every given frequency, the steps between each measured point and how many periods are skipped in the beginning of the frequency sweep in order to synchronize the device, respectively.

During the experiments a faulty power amplifier had to be switched out. One of the capacitors was damaged and because of that the unit could not function properly, it could not generate the proper measuring signals. After the repairs the device started to function. At first the results were very inaccurate. With trying out different amplitudes and different setup parameters more and more accurate results were achieved. In order to measure accurately, higher amplitudes were used for the measuring signals alongside with a higher averaging count (average=30 compared to the BioLogic instrument, which only uses N_a=3). The measurements were carried out in the frequency range from 50 kHz to 50 mHz. This range was used partially because of the faster measurement times and partially because of the experimental device (the highest frequency setting on the device is 50 kHz). The BioLogic instrument completed these measurements under five minutes; however the experimental device needed more time (around fifteen minutes), because of the much higher average count.

The device in its current state functions and is able to use both measuring methods. In order to precisely determine the amplitudes for the measuring signals, thus reducing the differences between the two instruments, further experiments are needed. Other improvements would include the addition of a more practical user interface for setting up the measurements and streamline the work with the measured data. The versatility and the relatively easy handling of the device are amongst the biggest advantages. However the greatest advantage lies in the price/quality (features) ratio, for small scale applications it is exceptional.

LITERATURE

[1] CHEMICAL REVIEW, Before Li Ion Batteries. [online]. [cit. 2019-05-20]. Available from: https://pubs.acs.org/doi/10.1021/acs.chemrev.8b00422

[2] Cell Chemistries – How Batteries Work. [online]. [cit. 2019-05-20]. Available from: http://www.mpoweruk.com/chemistries.htm

[3] How do Lithium Batteries Work?. [online]. [cit. 2019-05-20]. Available from: http://batteryuniversity.com/learn/article/lithium_based_batteries

[4] Is Lithium-ion the Ideal Battery?. [online]. [cit. 2019-05-20]. Available from: http://batteryuniversity.com/learn/article/is_lithium_ion_the_ideal_battery

[5] Lithium-ion battery. In: *Wikipedia: the free encyclopedia* [online]. San Francisco (CA): Wikimedia Foundation, 2001- [cit. 2019-05-20]. Available from: https://en.wikipedia.org/wiki/Lithium-ion_battery

[6] PISTOIA, G. *Lithium-ion batteries: advances and applications*. Amsterdam: Elsevier, 2014. ISBN 0444595139.

[7] Designing Applications with Li-ion Batteries. [online]. [cit. 2019-05-20]. Available from: http://www.richtek.com/battery-management/en/designing-liion.html

[8] RAHN, Christopher D. *Battery systems engineering*. Chichester, West Sussex, United Kingdom: John Wiley & Sons Ltd., Publication, 2013. ISBN 9781119979500.

[9] ŠIKUDA, M. *Záporné elektrodové materiály v lithium-iontovém akumulátoru.* Brno: Vysoké učení technické v Brně, Fakulta elektrotechniky a komunikačních technologií, 2015. 79 s. Vedoucí diplomové práce Ing. Jiří Libich

[10] TATARKOVIČ, Michal, BRONCOVÁ Gabriela a KRONĎÁK Martin. ELEKTROIMPEDANČNÍ SPEKTROSKOPIE A JEJÍ VYUŽITÍ V CHEMICKÉ ANALÝZE. Chemické listy [online]. 2011, č. 106, s. 1067-1074, 2.12.2011 [cit. 2019-05-20]. Available from: http://www.chemicke-listy.cz/docs/full/2012_11_1067-1074.pdf

[11] Basics of Electrochemical Impedance Spectroscopy [online]. GAMRI Instruments [cit. 2019-05-20]. Available from: https://www.gamry.com/application-notes/EIS/basics-of-electrochemical-impedance-spectroscopy/

[12] In-situ characterization of EIS [online]. [cit. 2019-05-20]. Available from: https://nptel.ac.in/courses/103102015/fuel%20cell%20characterization/in%20situ%20characterization.html

[13] 14-Bit, Single Channel, Serial Interface, Multiplying Digital-to-Analog Converter [online]. [cit. 2019-05-20]. Available from: http://www.ti.com/product/DAC8801/description

[14] Reinforced Isolated Modulator With ±50mV Input and CMOS Interface [online]. [cit. 2019-05-20]. Available from: http://www.ti.com/product/AMC1305M05/description?jktype=didyoumean

[15] The 32L4R9IDISCOVERY kit [online]. [cit. 2019-05-20]. Available from: https://www.st.com/content/st_com/en/products/evaluation-tools/product-evaluation-

tools/mcu-mpu-eval-tools/stm32-mcu-mpu-eval-tools/stm32-discovery-kits/32l4r9idiscovery.html#overview

[16] Lithium-ion battery models: a comparative study and a model-based powerline communication [online]. [cit. 2019-05-20]. Available from: https://www.researchgate.net/publication/319983930_Lithium-ion_battery_models_A_comparative_study_and_a_model-based_powerline_communication

[17] Study on electrochemical impedance spectrum of C-LiFePO 4 power battery [online]. [cit. 2019-05-20]. Available from: https://www.researchgate.net/publication/329627744_Study_on_electrochemical_impedance_spectrum_of_C-LiFePO_4_power_battery

[18] Datasheet Panasonic NCR18650B [online]. [cit. 2019-05-20]. Available from: https://www.batteryspace.com/prod-specs/NCR18650B.pdf

[19] Datasheet Panasonic NCR18650F [online]. [cit. 2019-05-20]. Available from: https://www.omnitron.cz/download/datasheet/NCR-18650F.pdf

List of appendices

The enclosed CD for the printed version or the packaged zip file for the online version has the following folders containing the Excel documents with the measured data:

- PEIS_GEIS_soldered
  - BioLogic
    - charged
    - discharged
  - Experimental device
    - charged
    - discharged
- PEIS_GEIS_with_clips
  - BioLogic
    - charged
    - discharged
  - Experimental device
    - charged
    - discharged

The printed version only shows examples of the tables and graphs saved as digital appendices.

Table 7.1 Panasonic NCR 18650 B, GEIS, charged

f [Hz]	U_{AC} [V]	I_{AC} [A]	φ [°]	Real Z [Ω]	Imaginary Z [Ω]
5,00E+04	9,11E-02	1,00E+00	-3,83E+01	7,15E-02	-5,64E-02
3,43E+04	9,23E-02	1,18E+00	-3,20E+01	6,62E-02	-4,14E-02
2,31E+04	7,59E-02	1,11E+00	-2,55E+01	6,19E-02	-2,96E-02
1,58E+04	6,59E-02	1,05E+00	-1,92E+01	5,96E-02	-2,08E-02
1,08E+04	6,16E-02	1,04E+00	-1,48E+01	5,75E-02	-1,52E-02
7,32E+03	5,82E-02	1,02E+00	-9,92E+00	5,64E-02	-9,87E-03
5,00E+03	5,67E-02	1,01E+00	-6,81E+00	5,58E-02	-6,66E-03
3,40E+03	5,63E-02	1,01E+00	-3,71E+00	5,58E-02	-3,62E-03
2,32E+03	5,63E-02	1,00E+00	-1,61E+00	5,60E-02	-1,57E-03
1,58E+03	5,68E-02	1,00E+00	9,96E-02	5,67E-02	9,86E-05
1,08E+03	5,74E-02	1,00E+00	9,22E-01	5,73E-02	9,23E-04
7,33E+02	5,81E-02	1,00E+00	1,88E+00	5,81E-02	1,90E-03
4,99E+02	5,89E-02	9,99E-01	2,31E+00	5,89E-02	2,38E-03
3,40E+02	5,98E-02	9,99E-01	2,52E+00	5,98E-02	2,63E-03
2,32E+02	6,07E-02	9,99E-01	2,61E+00	6,07E-02	2,77E-03
1,58E+02	6,14E-02	9,98E-01	2,73E+00	6,15E-02	2,93E-03
1,08E+02	6,23E-02	9,99E-01	2,66E+00	6,23E-02	2,89E-03
7,32E+01	6,32E-02	9,99E-01	2,53E+00	6,32E-02	2,79E-03
4,99E+01	6,39E-02	9,99E-01	2,42E+00	6,39E-02	2,70E-03
3,40E+01	6,46E-02	9,97E-01	2,04E+00	6,48E-02	2,31E-03
2,32E+01	6,50E-02	9,96E-01	1,76E+00	6,53E-02	2,00E-03
1,58E+01	6,54E-02	9,95E-01	1,64E+00	6,57E-02	1,88E-03
1,07E+01	6,58E-02	9,95E-01	1,40E+00	6,61E-02	1,61E-03
7,32E+00	6,62E-02	9,96E-01	1,17E+00	6,65E-02	1,35E-03
4,98E+00	6,66E-02	9,98E-01	1,12E+00	6,67E-02	1,30E-03
3,40E+00	6,69E-02	1,00E+00	9,22E-01	6,69E-02	1,08E-03
2,31E+00	6,70E-02	9,98E-01	9,72E-01	6,71E-02	1,14E-03
1,58E+00	6,74E-02	1,00E+00	8,24E-01	6,73E-02	9,67E-04
1,07E+00	6,76E-02	1,00E+00	9,87E-01	6,76E-02	1,17E-03
7,31E-01	6,79E-02	1,00E+00	1,05E+00	6,78E-02	1,25E-03
4,98E-01	6,80E-02	1,00E+00	1,33E+00	6,79E-02	1,57E-03
3,39E-01	6,82E-02	1,00E+00	1,42E+00	6,81E-02	1,69E-03
2,31E-01	6,84E-02	1,00E+00	1,55E+00	6,83E-02	1,85E-03

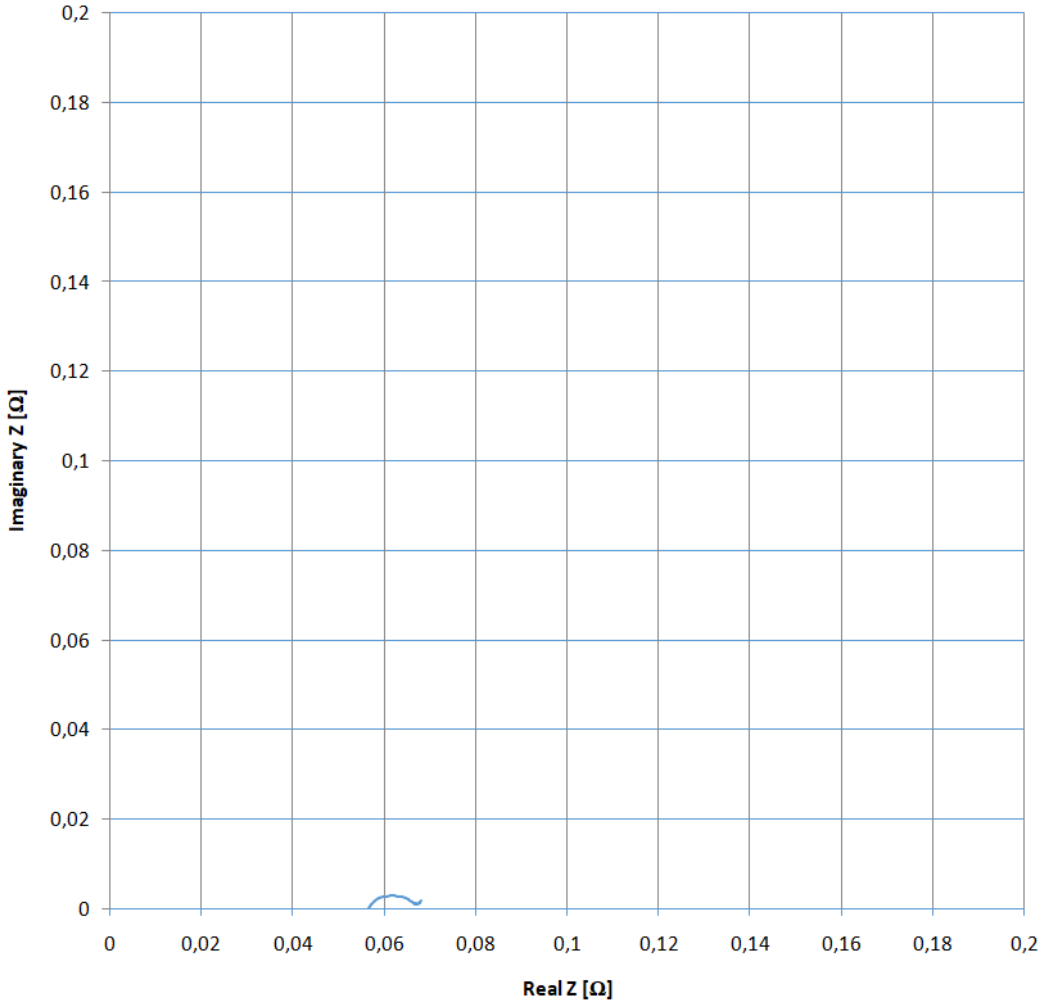

Figure 7.1 Panasonic NCR 18650 B, Nyquist Plot, GEIS, charged

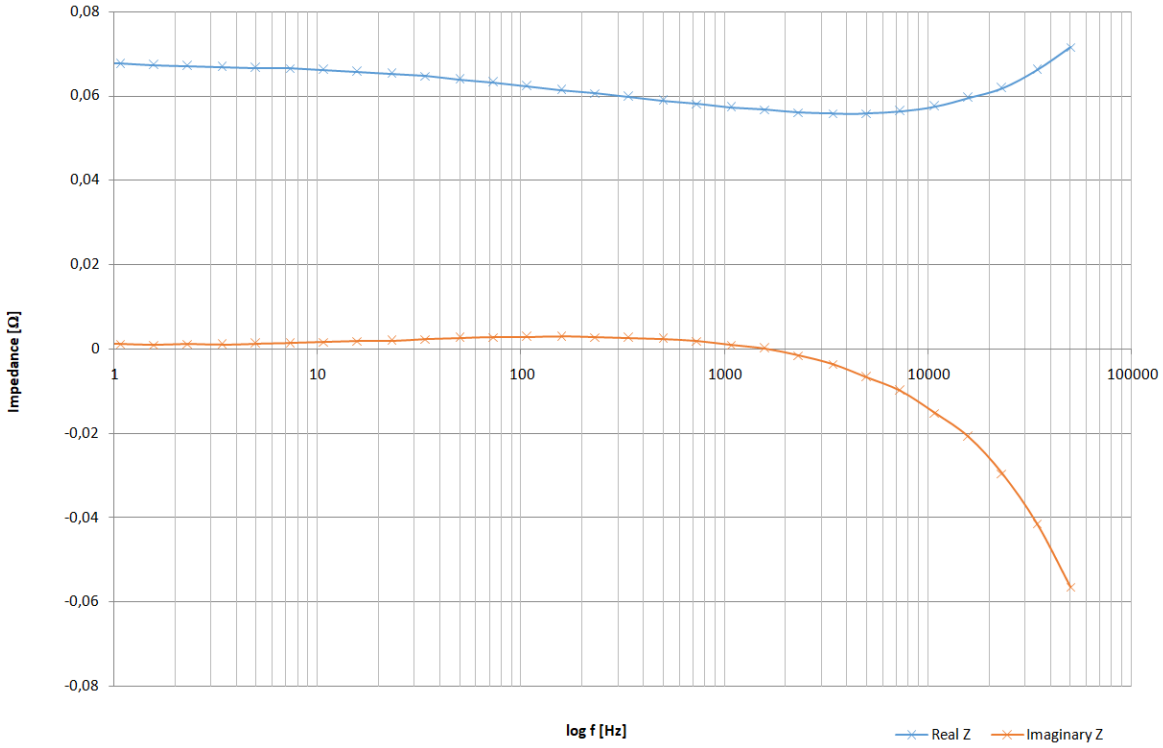

Figure 7.2 Panasonic NCR 18650 B, Bode Plot for the Impedance, GEIS, charged

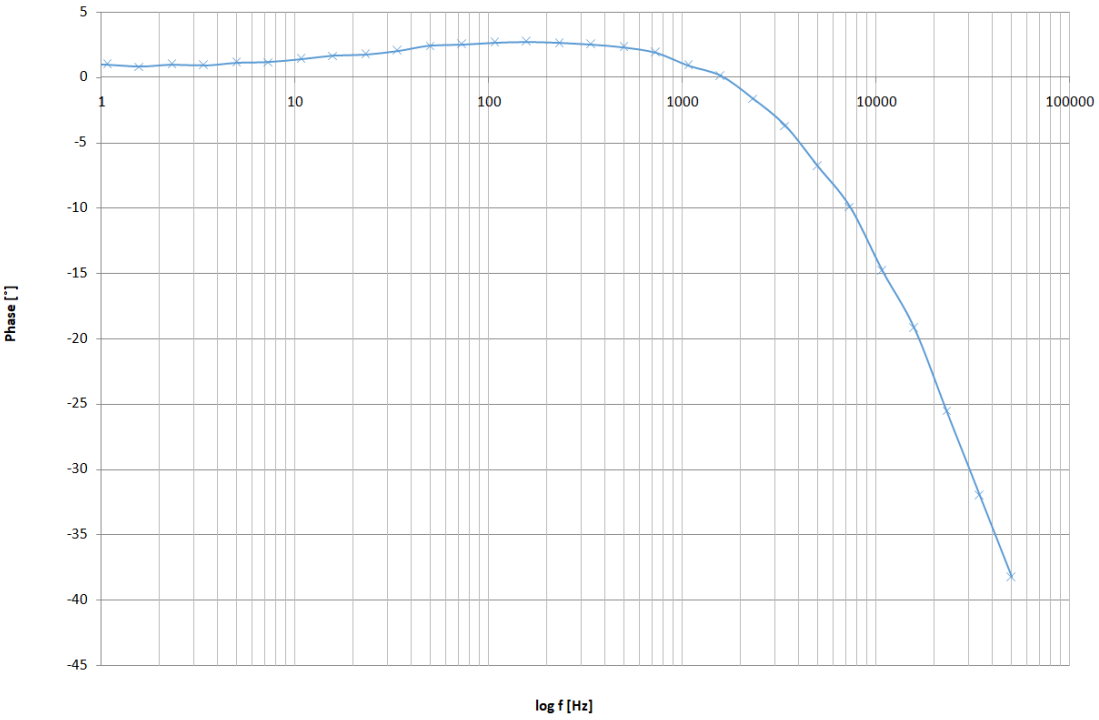

Figure 7.3 Panasonic NCR 18650 B, Bode Plot for the phase, GEIS, charged

Table 7.2 Panasonic NCR 18650 B, GEIS, discharged

f [Hz]	U_{AC} [V]	I_{AC} [A]	φ [°]	Real Z [Ω]	Imaginary Z [Ω]
5,00E+04	1,01E-01	1,00E+00	-4,02E+01	7,71E-02	-6,52E-02
3,43E+04	1,01E-01	1,18E+00	-3,36E+01	7,10E-02	-4,71E-02
2,31E+04	8,23E-02	1,10E+00	-2,64E+01	6,68E-02	-3,32E-02
1,58E+04	7,11E-02	1,04E+00	-1,96E+01	6,42E-02	-2,29E-02
1,08E+04	6,69E-02	1,04E+00	-1,48E+01	6,25E-02	-1,65E-02
7,32E+03	6,32E-02	1,02E+00	-9,92E+00	6,14E-02	-1,07E-02
5,00E+03	6,23E-02	1,01E+00	-6,00E+00	6,14E-02	-6,46E-03
3,40E+03	6,20E-02	1,01E+00	-3,52E+00	6,16E-02	-3,79E-03
2,32E+03	6,21E-02	1,00E+00	-1,09E+00	6,19E-02	-1,18E-03
1,58E+03	6,26E-02	1,00E+00	2,46E-01	6,25E-02	2,68E-04
1,08E+03	6,33E-02	1,00E+00	1,50E+00	6,33E-02	1,66E-03
7,33E+02	6,44E-02	1,00E+00	2,12E+00	6,43E-02	2,38E-03
4,99E+02	6,53E-02	9,99E-01	2,69E+00	6,52E-02	3,06E-03
3,40E+02	6,63E-02	9,99E-01	3,08E+00	6,62E-02	3,56E-03
2,32E+02	6,73E-02	9,99E-01	3,26E+00	6,73E-02	3,83E-03
1,58E+02	6,83E-02	9,98E-01	3,40E+00	6,83E-02	4,06E-03
1,08E+02	6,95E-02	9,99E-01	3,31E+00	6,95E-02	4,01E-03
7,32E+01	7,05E-02	9,99E-01	3,42E+00	7,05E-02	4,21E-03
4,99E+01	7,15E-02	9,98E-01	3,55E+00	7,15E-02	4,44E-03
3,40E+01	7,24E-02	9,97E-01	3,47E+00	7,24E-02	4,39E-03
2,32E+01	7,33E-02	9,95E-01	3,65E+00	7,35E-02	4,69E-03
1,58E+01	7,42E-02	9,94E-01	3,87E+00	7,44E-02	5,04E-03
1,07E+01	7,52E-02	9,95E-01	4,23E+00	7,54E-02	5,58E-03
7,32E+00	7,63E-02	9,95E-01	4,88E+00	7,64E-02	6,52E-03
4,98E+00	7,76E-02	9,97E-01	5,77E+00	7,74E-02	7,82E-03
3,40E+00	7,93E-02	9,99E-01	6,79E+00	7,88E-02	9,38E-03
2,31E+00	8,13E-02	9,96E-01	8,46E+00	8,07E-02	1,20E-02
1,58E+00	8,46E-02	9,99E-01	1,02E+01	8,34E-02	1,51E-02
1,07E+00	8,93E-02	9,96E-01	1,18E+01	8,78E-02	1,84E-02
7,31E-01	9,53E-02	9,96E-01	1,31E+01	9,32E-02	2,17E-02
4,98E-01	1,02E-01	9,95E-01	1,34E+01	1,00E-01	2,38E-02
3,39E-01	1,09E-01	9,95E-01	1,30E+01	1,07E-01	2,46E-02
2,31E-01	1,16E-01	9,95E-01	1,16E+01	1,14E-01	2,34E-02

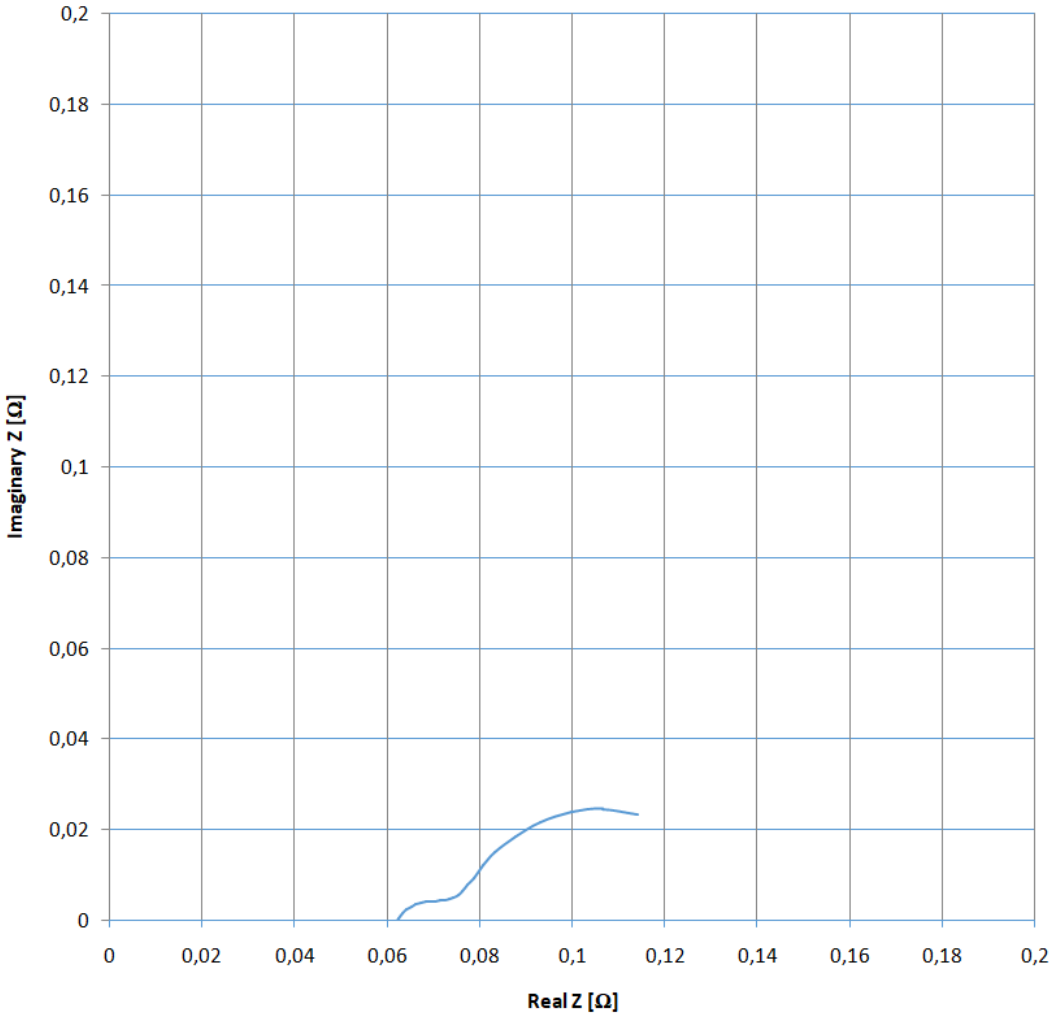

Figure 7.4 Panasonic NCR 18650 B, Nyquist Plot, GEIS, discharged

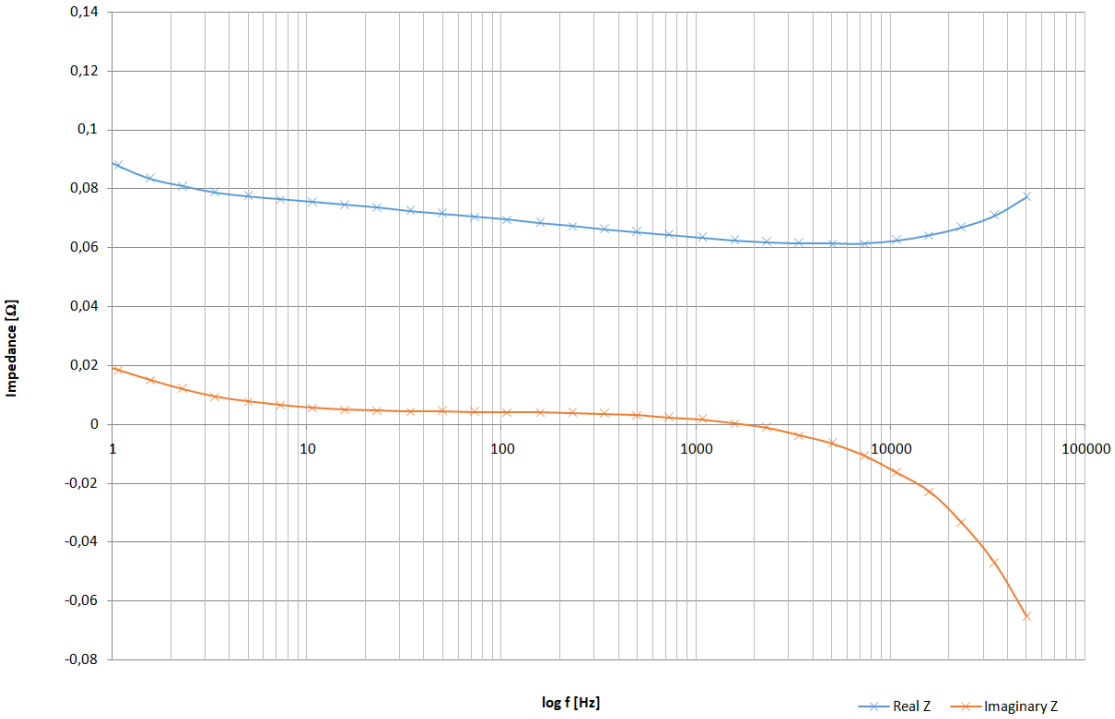

Figure 7.5 Panasonic NCR 18650 B, Bode Plot for the Impedance, GEIS, discharged

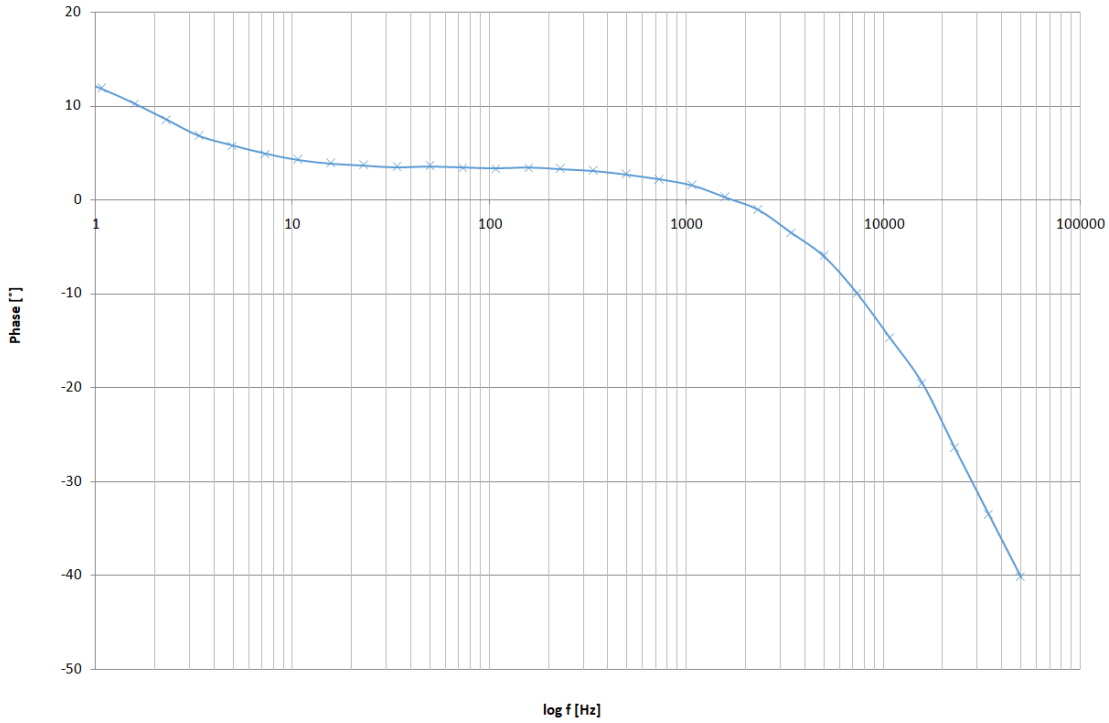

Figure 7.6 Panasonic NCR 18650 B, Bode Plot for the phase, GEIS, discharged